Macromolecules

ARTICLE

pubs.acs.org/Macromolecules

Polyelectrolytes in Salt Solutions: Molecular Dynamics Simulations

Jan-Michael Y. Carrillo and Andrey V. Dobrynin*

Polymer Program, Institute of Materials Science and Department of Physics, University of Connecticut, Storrs, Connecticut 06269, United States

ABSTRACT: We present results of the molecular dynamics simulations of salt solutions of polyelectrolyte chains with number of monomers $N = 300$. Polyelectrolyte solutions are modeled as an ensemble of bead−spring chains of charged Lennard-Jones particles with explicit counterions and salt ions. Our simulations show that in dilute and semidilute polyelectrolyte solutions the electrostatic induced chain persistence length scales with the solution ionic strength as $I^{-1/2}$. This dependence of the chain persistence length is due to counterion condensation on the polymer backbone. In dilute polyelectrolyte solutions the chain size decreases with increasing the salt concentration as $R \propto I^{-1/5}$. This is in agreement with the scaling of the chain persistence length on the solution ionic strength, $l_p \propto I^{-1/2}$. In semidilute solution regime at low salt concentrations the chain size decreases with increasing polymer concentration, $R \propto c_p^{-1/4}$, while at high salt concentrations we observed a weaker dependence of the chain size on the solution ionic strength, $R \propto I^{-1/8}$. Our simulations also confirmed that the peak position in the polymer scattering function scales with the polymer concentration in dilute polyelectrolyte solutions as $c_p^{1/3}$. In semidilute polyelectrolyte solutions at low salt concentrations the location of the peak in the scattering function shifts toward the large values of $q^* \propto c_p^{1/2}$ while at high salt concentrations the peak location depends on the solution ionic strength as $I^{-1/4}$. Analysis of the simulation data throughout the studied salt and polymer concentration ranges shows that there exist general scaling relations between multiple quantities $X(I)$ in salt solutions and corresponding quantities $X(I_0)$ in salt-free solutions, $X(I) = X(I_0)(I/I_0)^{\beta}$. The exponent $\beta = -1/2$ for chain persistence length l_p, $\beta = 1/4$ for solution correlation length ξ, and $\beta = -1/5$ and $\beta = -1/8$ for chain size R in dilute and semidilute solution regimes, respectively.

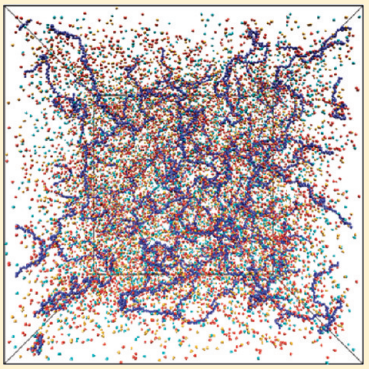

1. INTRODUCTION

Polyelectrolytes are macromolecules with ionizable groups. In aqueous solutions charged groups dissociate, leaving charges on the chain and releasing counterions into solution. Common polyelectrolytes include poly(acrylic acid) and poly(methacrylic acid) and their salts, poly(styrenesulfonate), DNA, RNA, and other polyacids and polybases.[1−9]

Polyelectrolytes play an important role in a diverse number of fields ranging from materials science and colloids to biophysics. These polymers are used as rheology modifiers, adsorbents, coatings, biomedical implants, colloidal stabilizing agents, and suspending agents for pharmaceutical delivery systems.

Electrostatic interactions between charges lead to the rich behavior of these polymeric systems (see for review refs 1−5 and 7). For example, in salt-free polyelectrolyte solutions the electrostatic interactions between charged groups on the polymer backbone result in a strong chain elongation with chain size scaling almost linearly with the chain degree of polymerization. Because of this strong dependence of the chain size on the chain degree of polymerization, the crossover to semidilute polyelectrolyte solution regime occurs at much low polymer concentrations than in solutions of neutral polymers.[1,5,6,8,10] The main contribution to the osmotic pressure in polyelectrolyte solutions comes from the ionic component.[9,11−15] Polyelectrolyte conformations are sensitive to the solvent quality for the polymer backbone. In poor solvent conditions for the polymer backbone a polyelectrolyte chain forms an unusual necklace-like structure of dense polymeric beads connected by strings of monomers.[1,16−30] Similar necklace-like structure can be formed in hydrophobically modified polyelectrolytes in which a hydrophobic side chains are attached to the polyelectrolyte backbone.[31]

Addition of salt leads to screening of the electrostatic interactions between ionized groups reducing the polyelectrolyte effect (see for review refs 1 and 2). At high salt concentrations properties of polyelectrolyte solutions are similar to those of neutral polymers with effective second virial coefficient between monomers which strength is determined by the salt concentration and by the fraction of the ionized groups along the polymer backbone. While there is a significant number of experimental studies of polyelectrolytes in salt solutions (see for review refs 1, 2, and 6) the computational studies of the salt effect on the properties of polyelectrolyte solutions are lagging behind.[3,32−41] The computer simulations of the polyelectrolyte solutions in the presence of salt were limited to investigation of the salt effect on the single chain properties.[33−37] The salt ions in these simulations were taken into account either explicitly or implicitly by modeling the screening effect of the salt ions by representing the electrostatic interactions between charged monomers by the

Received: April 5, 2011
Revised: June 6, 2011
Published: June 30, 2011

ACS Publications © 2011 American Chemical Society

Debye−Huckel potential. A comparison between simulations with explicit and implicit salt ions was performed by Stevens and Plimpton.[41] Simulations with explicit salt ions[35−37] were restricted to a dilute solution regime where the intrachain electrostatic interactions dominate over interchain ones and system behavior can be judged from single chain simulations. The general conclusion of these simulations was that the salt ions screen electrostatic interactions, resulting in reduction of the chain size with increasing the salt concentration. Unfortunately, the studied interval of salt concentrations prevented identification of pure scaling regimes in chain size dependence on the solution ionic strength.

In this paper we use molecular dynamics simulations to study effect of the salt concentration on the polyelectrolyte solution properties in dilute and semidilute solution regimes. We elucidated the effect of salt concentration on the chain size, solution correlation length, chain overlap concentration, counterion condensation on the polymer backbone, and solution pressure. To establish the effect of the chain rigidity on the solution properties, we have performed simulations of polyelectrolyte chains with different bending rigidities.

2. MOLECULAR DYNAMICS SIMULATIONS

We performed molecular dynamics simulations[42] of polyelectrolyte solutions in dilute and semidilute solution regimes in the presence of salt. The simulation details are given in Appendix A, below we briefly describe our model. In our simulations we used a coarse-grained representation of polyelectrolyte chains, counterions, and salt ions.[32,41,43,44] In this representation monomers and small ions are modeled by the charged Lennard-Jones particles with diameter σ. The value of the Lennard-Jones interaction parameter ε_{LJ} for polymer−polymer pairs was set to 0.3 k_BT (where k_B is the Boltzmann constant and T is the absolute temperature). The selection of the parameters for the LJ interaction potential between polymer−ion pairs corresponds to pure repulsive interactions (see Appendix A for details). The connectivity of the monomers into a polymer chain was maintained by the FENE potential. To introduce a chain bending rigidity, we have imposed a bending potential between neighboring along the polymer backbone bond vectors. The value of the chain bending constant was set to $K = 0$, 3, and 6. The chain degree of polymerization was equal to $N = 300$ for all simulations. The solvent was treated implicitly as a medium with the dielectric permittivity ε. All monomers on the polymer backbone were charged. This corresponds to the fraction of charged monomers $f = 1$. The electrostatic interactions between all charges in a system were treated explicitly through the Coulomb potential. The value of the Bjerrum length was $l_B = 1.0\ \sigma$, where $l_B = e^2/\varepsilon k_BT$ is defined as the length scale at which the Coulomb interaction between two elementary charges, e, in a medium with the dielectric constant, ε, is equal to the thermal energy, k_BT. In our simulations we varied the polymer concentration, c_p, between 10^{-4} and 10^{-1} σ^{-3} and salt concentration, c_s, between 5×10^{-5} and 5×10^{-2} σ^{-3}. The simulations were performed in the NVT ensemble with periodic boundary conditions. A mapping of coarse-grained parameters onto real polymeric systems is given in Appendix A.

3. OVERLAP CONCENTRATION

We begin discussion of properties of polyelectrolyte solutions by establishing location of the crossover between dilute and semidilute solution regimes by determining a chain overlap concentration c_p^*.[45,46] In the dilute solution regime, $c_p < c_p^*$, the polyelectrolyte chains are separated from each other by average distances D larger than their size. At such low polymer concentrations the intrachain electrostatic interactions and interactions with the surrounding polyelectrolyte chain ions determine the chain conformations. At polymer concentrations higher than the overlap concentration, $c_p > c_p^*$, the interchain electrostatic interactions with surrounding chains control chain conformations.

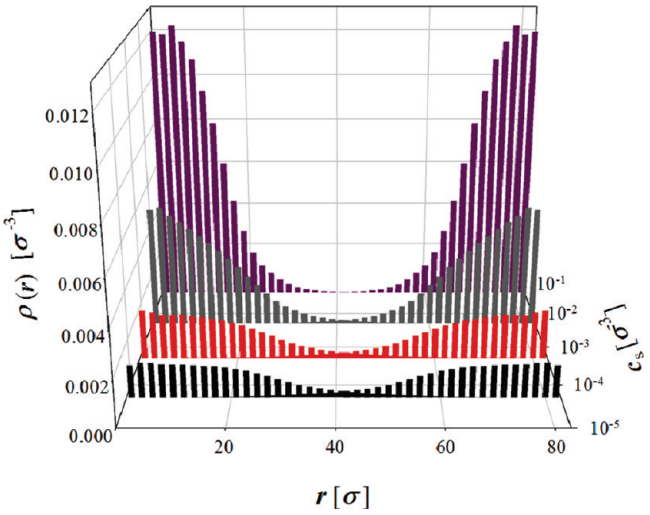

Figure 1. Monomer radial density distribution, $\rho(r)$, with respect to chain center of mass along the direction connecting centers of mass of two neighboring chains located at $r = 0$ and $r = D$ for fully charged polyelectrolyte chains with the degree of polymerization $N = 300$, chain bending constant $K = 0$, at polymer concentration $c_p = 10^{-3}\ \sigma^{-3}$ and at different salt concentrations: $c_s = 5 \times 10^{-5}\ \sigma^{-3}$ (black bars), $c_s = 5 \times 10^{-4}\ \sigma^{-3}$ (red bars), $c_s = 5 \times 10^{-3}\ \sigma^{-3}$ (gray bars), and $c_s = 5 \times 10^{-2}\ \sigma^{-3}$ (magenta bars).

Figure 1 shows radial distribution of the monomer density with respect to the chain center of mass along the line connecting centers of mass of two neighboring polyelectrolyte chains. This distribution function of the monomer density was obtained by averaging the monomer density within spherical shells of size r and thickness $\Delta = 2\sigma$ during the production run. The average distance between chain centers of mass D was calculated by using a 3-D tessellation procedure. This allowed us to determine the list of the nearest-neighbor chains and to obtain distances between them during simulation runs. These distances were averaged over all system configurations. This analysis shows that the average distance between chains is on the order of $D \approx (6N/\pi c_p)^{1/3}$. In semidilute solution regime the monomer clouds surrounding chain center of mass overlap (see Figure 1). With increasing the salt concentration the monomer density distribution around the chain center of mass shrinks, eventually leading to nonoverlapping monomer clouds. The overlap between monomer clouds begins at $D \approx 4\langle R_g^2\rangle^{1/2}$ where the mean-square chain radius of gyration is defined as

$$\langle R_g^2\rangle = \frac{1}{N^2}\langle \sum_{i<j}^{N} (\vec{r}_i - \vec{r}_j)^2\rangle \qquad (1)$$

$\vec{r}_i$ is the radius vectors of the ith monomer on the polymer backbone and average is calculated over all chain configurations. Note that at these separations between chain centers of mass the average monomer density in the overlapping region is less than 1% of the maximum value of the monomer density. These monomer densities are lower than the density fluctuation values. At separations between chains on the order of $D \approx 3\langle R_g^2\rangle^{1/2}$ the monomer density in the overlap region is larger than the 5% of its maximum value and is

dx.doi.org/10.1021/ma2007943 |Macromolecules 2011, 44, 5798–5816

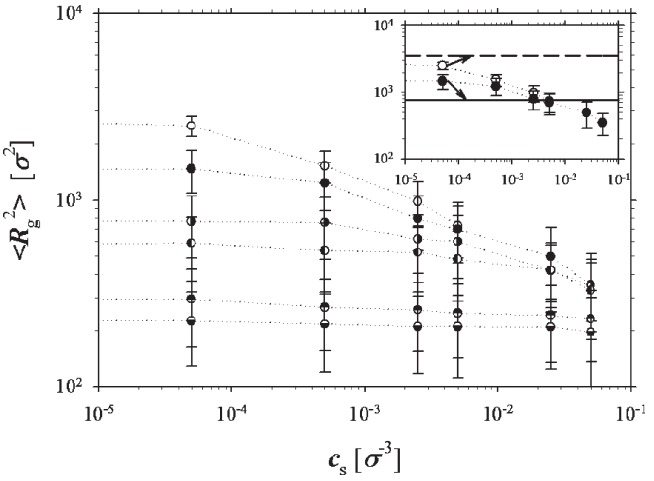

Figure 2. Dependence of the mean-square radius of gyration $\langle R_g^2 \rangle$ on salt concentration for fully charged polyelectrolyte chains with the degree of polymerization $N = 300$, chain bending constant $K = 0$ at different polymer concentrations: $c_p = 10^{-4}\,\sigma^{-3}$ (open circles), $c_p = 10^{-3}\,\sigma^{-3}$ (filled circles), $c_p = 5 \times 10^{-3}\,\sigma^{-3}$ (half-filled circles, right), $c_p = 10^{-2}\,\sigma^{-3}$ (half-filled circles, left), $c_p = 5 \times 10^{-2}\,\sigma^{-3}$ (half-filled circles, top), and $c_p = 10^{-1}\,\sigma^{-3}$ (half-filled circles, bottom). Inset shows location of the overlap concentration evaluated from $\langle R_g^2 \rangle = D^2/9$, which separates dilute and semidilute solution regimes for two polymer concentrations $c_p = 10^{-4}\,\sigma^{-3}$ (dashed line) and $c_p = 10^{-3}\,\sigma^{-3}$ (solid line).

larger than the density fluctuations. We selected polymer concentration at which the distance between chain's center of mass $D \approx 3\langle R_g^2 \rangle^{1/2}$ as a crossover polymer concentration to the semidilute solution regime c_p^*. Note that this selection is not unique. For example, one can determine the chain overlap concentration as concentration at which the distance between chains D is on the order of the square-root of the mean square end-to-end distance, $D \approx (\langle R_e^2 \rangle)^{1/2}$. This will lead to a different numerical coefficient in the expression for an overlap concentration as a function of the chain degree of polymerization.

In Figure 2, we plot dependence of the mean-square value of the chain radius of gyration on the salt concentration c_s for polymer concentration c_p varied between 10^{-4} and $0.1\,\sigma^{-3}$. The horizontal lines on this figure correspond to the following equation $D^2/9 \approx (2/9\pi)^{2/3} c_p^{-2/3}$. At overlap concentration the polymer density is on the order of

$$c_p \approx c_p^* \approx \frac{2N}{9\pi \langle R_g^2 \rangle^{3/2}} \qquad (2)$$

It follows from this plot that for our lowest polymer concentration $c_p = 10^{-4}\,\sigma^{-3}$ the system is just below the chain overlap concentration. For polymer concentration $c_p = 10^{-3}\,\sigma^{-3}$ the salt-free solution and salt solutions with $c_s < 10^{-3}\,\sigma^{-3}$ are in a semidilute solution regime while polyelectrolyte solutions with $c_s > 10^{-3}\,\sigma^{-3}$ are in a dilute solution regime. Polyelectrolyte solutions with polymer concentrations $c_p > 10^{-3}\,\sigma^{-3}$ are in semidilute solution regime throughout the entire interval of the salt concentrations studied in our simulations. Figure 3 shows location of the dilute and semidilute solution regimes as a function of the polymer and salt concentrations.

Note that with increasing a chain bending constant K the size of the polyelectrolyte chain increases. The analysis of the simulation data for $K = 3$ and 6 shows that all these systems show a slightly narrower interval of polymer and salt concentrations corresponding to a dilute solution regime.

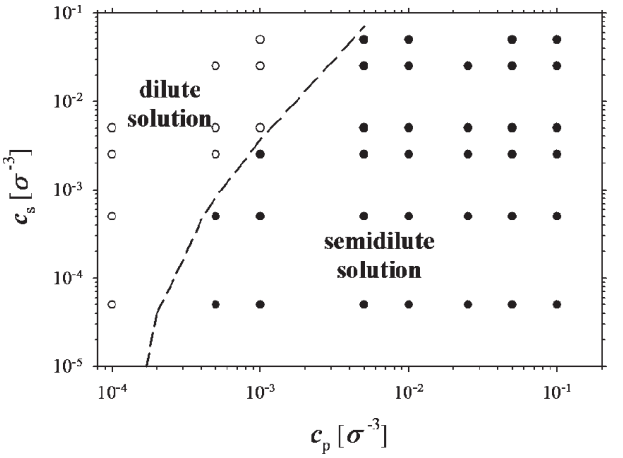

Figure 3. Diagram of different solution regimes. Filled symbols correspond to semidilute solution regime, and open symbols show dilute solution regime.

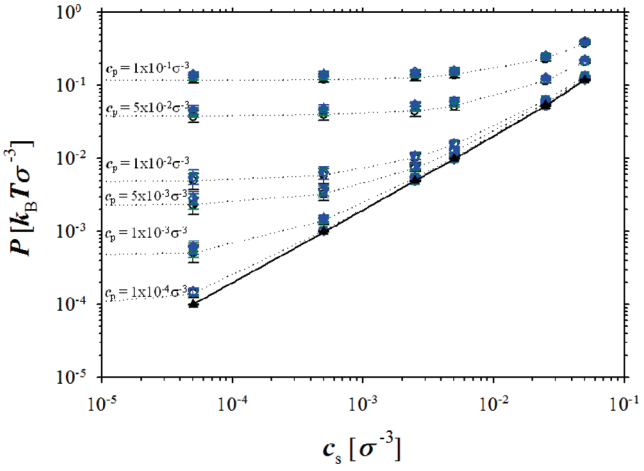

Figure 4. Dependence of the system pressure P on salt concentration for fully charged polyelectrolyte chains with the degree of polymerization $N = 300$, different values of the chain bending constants: $K = 0$ (black circles), $K = 3$ (green squares), and $K = 6$ (blue rhombs); and at different polymer concentrations. Black triangles with solid line show pressure dependence on salt concentration in polymer-free systems.

4. SYSTEM PRESSURE AND OSMOTICALLY ACTIVE COUNTERIONS

In polyelectrolyte solutions the pressure is dominated by contribution from small ions.[1−7,15,47,48] Figure 4 shows dependence of the system pressure P on the salt concentration at different polymer concentrations. At low salt concentrations the system pressure has a plateau. The magnitude of the plateau shifts toward larger pressure values with increasing the polymer concentration. At high salt concentrations, $2c_s > c_p$, the system pressure is a linear function of the salt concentration, indicating that it is controlled by the pressure generated by salt ions. For systems with polymer concentrations $c_p < 5 \times 10^{-2}\,\sigma^{-3}$ in the high salt concentration regime the pressure curves approach those obtained from simulations of the polymer-free systems. The crossover between high and low salt concentration regimes shifts toward high salt concentrations with increasing the polymer concentration and occurs when the

dx.doi.org/10.1021/ma2007943 |*Macromolecules* 2011, 44, 5798–5816

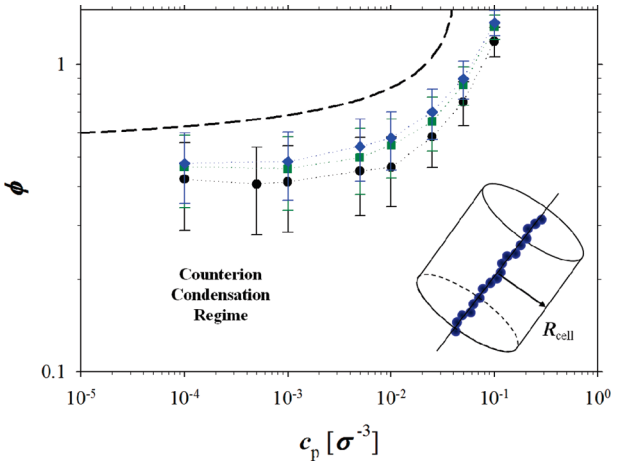

Figure 5. Dependence of the osmotic coefficient ϕ on polymer concentration in salt-free solutions of fully charged polyelectrolyte chains with the degree of polymerization $N = 300$ and different values of the chain bending constants: $K = 0$ (black circles), $K = 3$ (green squares), and $K = 6$ (blue rhombs). The dashed line shows the boundary of the counterion condensation regime of the Katchalsky's cell model (see text for details). Inset shows a schematic representation of a chain in the Katchalsky's cell model.

salt concentration becomes on the order of half of the polymer concentration, $c_P/2$. It also follows from Figure 4 that the data sets are shifted by a factor which magnitude depends on polymer concentration. To establish a shift factor, we plot dependence of the osmotic coefficient

$$\phi = f^* = \frac{P}{k_B T c_p} \tag{3}$$

in salt-free solutions ($c_s = 0$) on polymer concentration c_p (see Figure 5). Note that only in salt-free solutions the system pressure is equivalent to the osmotic pressure of the system. The value of the osmotic coefficient in salt-free solutions is equal to the faction f^* of the osmotically active counterions.[1,5,13,15,47] In some publications the osmotically active counterions are referred to as "free" counterions that can explore the system volume and provide contribution to the system pressure (see for review ref 1). One can also think of the fraction of osmotically active counterions f^* as a counterion activity coefficient. At polymer concentrations $c_p < 10^{-2}\,\sigma^{-3}$ the fraction of the osmotically active counterions f^* is constant. It begins to increase with increasing the polymer concentration for $c_p > 10^{-2}\,\sigma^{-3}$. At polymer concentration $c_p = 0.1\,\sigma^{-3}$ the value of f^* is larger than unity, indicating that the polymeric part of the system pressure start to provide a sizable contribution to the system pressure (see for details refs 1 and 15).

Following ref 15 we can explain results of Figure 5 by using Katchalsky's cell model.[49,50] In the framework of this approach each polyelectrolyte chain locally is approximated by a rod surrounded by a cylindrical cell with size R_{cell} (see inset in Figure 5). The distribution of electrostatic potential throughout the cell is obtained by solving nonlinear Poisson–Boltzmann equation (see for details refs 1 and 15). According to Katchalsky's cell model, the value of the osmotic coefficient is equal to

$$\phi_{cell} = \frac{1+\alpha^2}{2\gamma_0} \tag{4}$$

where parameter α satisfies the following nonlinear equation

$$\tan\left(2\alpha \log\left(\frac{R_{cell}}{\sigma}\right)\right) = \frac{2(2\phi_{cell}-1)\alpha}{(2\phi_{cell}-1)^2-\alpha^2} \tag{5}$$

and parameter γ_0 is equal to the ratio of the Bjerrum length l_B to the projection distance between charged monomers d_c on the local chain orientation direction, $\gamma_0 = l_B/d_c$. The parameter γ_0 is also known as Manning–Oosawa counterion condensation parameter.[1] The critical value of the parameter $\gamma_0^{crit} = \log(R_{cell}/\sigma)/(1 + \log(R_{cell}/\sigma))$ determines a counterion condensation threshold. At $\gamma_0 = \gamma_0^{crit}$ the value of the parameter α is equal to zero. Equations 4 and 5 can be used to find values of the parameters α and γ_0 as a function of the system osmotic coefficient ϕ and cell size R_{cell}. Note that the cell size R_{cell} is related to the polymer concentration c_p and Manning–Oosawa parameter γ_0. The monomer concentration within a cylindrical cell is on the order of $c_p \approx (\pi R_{cell}^2 d_c)^{-1} \approx (\gamma_0/\pi R_{cell}^2 l_B)$. Solving it for R_{cell}, we can derive an expression for the cell size in terms of the polymer concentration c_p and Manning–Oosawa parameter γ_0, $R_{cell} \approx (\gamma_0/\pi l_B c_p)^{1/2}$. The dashed line in Figure 5 corresponds to the boundary of the counterion condensation regime (or saturated condensation regime in classification of refs 1 and 15), $\gamma_0 = \gamma_0^{crit}$, which was obtained by substituting into eq 4 $\alpha = 0$, $\gamma_0 = \gamma_0^{crit}$ and solving numerically the resultant nonlinear equation. As one can see, all our data points are inside the counterion condensation regime.

Solving eqs 4 and 5 for the values of the osmotic coefficient in the plateau regime, we obtain for average values of $\gamma_0 \approx 1.55$ ($K = 0$), $\gamma_0 \approx 1.41$ ($K = 3$), and $\gamma_0 \approx 1.31$ ($K = 6$). The value of the Manning–Oosawa counterion condensation parameter γ_0 increases with decreasing the chain bending rigidity K, indicating crumpling of more flexible chains at short length scales. This is manifested in shorter projection distances between charged monomers for flexible chains $d_c \approx 0.65\sigma$ ($K = 0$) in comparison with that for our stiffest chains with $K = 6$, $d_c \approx 0.77\sigma$.

With increasing the polymer concentration the distance between chains, R_{cell}, decreases, leading to increase of the value of the parameter α. This leads to increase of the value of the osmotic coefficient seen in Figure 5. The detailed comparison of the predictions of the Katchalsky's cell model with the results of the computer simulations of flexible and rodlike chains in salt-free solutions is given in ref 15. This analysis showed that the polymeric contribution begins to influence the system osmotic pressure at polymer concentrations $c_p > 0.05\,\sigma^{-3}$. In this concentration range the osmotic coefficient exceeds unity. The same trend is seen for our simulation data. Thus, to minimize polymeric contribution to the counterion activity coefficient, we only included data with $c_p \le 0.05\,\sigma^{-3}$ for our scaling analysis below.

It also worth pointing out that at salt concentration $c_s = 0.05\,\sigma^{-3}$ in the polymer-free case the system pressure is about 20% higher than one would expect from the ideal gas contribution of the salt ions. This points out that in addition to polymeric effects at high concentrations of polymers and salt ions the excluded volume interactions can also be an important factor leading in increase of the system pressure.[15,48]

At finite salt concentrations we can define a fraction of the osmotically active counterions or counterion activity coefficient as

$$f^* = \frac{P - 2k_B T c_s}{k_B T c_p} \tag{6}$$

It is important to point out that the definition of the fraction of osmotically active counterions given by eq 6 is only warranted in the concentration range where the pressure of the polyelectrolyte solutions is dominated by the linear terms in the virial expansion.

dx.doi.org/10.1021/ma2007943 |*Macromolecules* 2011, 44, 5798–5816

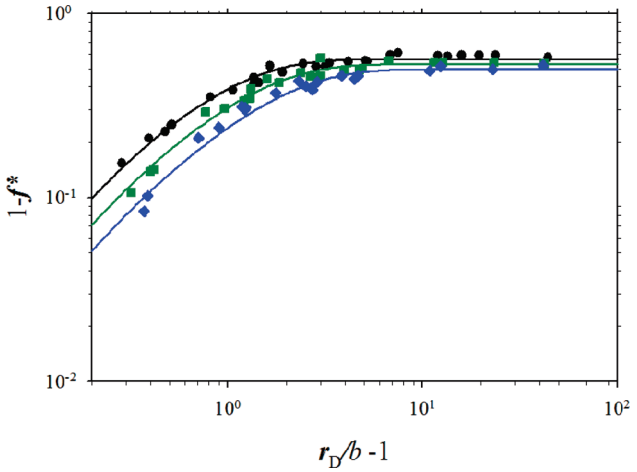

Figure 6. Dependence of fraction $1-f^*$ of the condensed counterions on the ratio of the Debye screening length to the bond length, r_D/b, for polyelectrolyte solutions of chains with $K = 0$ (black circles), $K = 3$ (green squares), and $K = 6$ (blue rhombs). The solid lines are the best fit to eq 8 with the values of the fitting parameters: $A = 0.566$, $B = 1.26$ for $K = 0$, $A = 0.532$, $B = 0.937$ for $K = 3$, and $A = 0.498$, $B = 0.710$ for $K = 6$. The data points correspond to polymer concentrations $c_p \leq 0.05\ \sigma^{-3}$ and salt concentrations $c_s < 0.05\ \sigma^{-3}$.

Analysis of the pressure data shows that we can represent the fraction of the condensed counterions (osmotically inactive counterions) $1-f^*$ in terms of the ratio of the Debye screening length

$$r_D^{-2} \equiv r_D^{-2}(c_p, c_s) = 4\pi l_B(f^* c_p + 2c_s) \quad (7)$$

to the average bond length b (see Figure 6). Note that in definition of the Debye screening length we only included osmotically active counterions by multiplying counterion concentration by activity coefficient, f^*. All data sets in Figure 6 have initial linear increase followed by saturation regime in the limit of large r_D/b ratios. Flexible chains with $K = 0$ have the highest value of the fraction of the condensed counterions $1-f^*$ in the plateau regime. This is in agreement with our observation that the flexible chains are more crumpled at short length scales in comparison with the chains having a finite K value. The simulation data points can be fitted by a function

$$1-f^* = A[1-\exp(-B(r_D(c_p, c_s)/b - 1))] \quad (8)$$

Using estimated values of the fraction f^* of the osmotically active counterions, we can collapse all data sets shown in Figure 4 into one universal plot. At low polymer and salt concentrations the system pressure is dominated by ideal gas-like contribution from osmotically active counterions and salt ions

$$P(I) \approx k_B T(f^* c_p + 2c_s) \approx P(I_0)\left(\frac{f^* c_p + 2c_s}{f_0^* c_p}\right)$$

$$\approx P(I_0)\frac{I}{I_0} \quad (9)$$

where $P(I_0) \approx k_B T c_p f_0^*$ is a pressure in a salt-free solution, f_0^* is the fraction of osmotically active counterions in a salt-free solution

$$I \equiv I(c_p, c_s) = f^* c_p + 2c_s \quad (10)$$

is the solution ionic strength, and I_0 is the solution ionic strength in salt-free solutions. Thus, one can conclude that the system pressure is a universal function of the ratio of the solution ionic strengths.

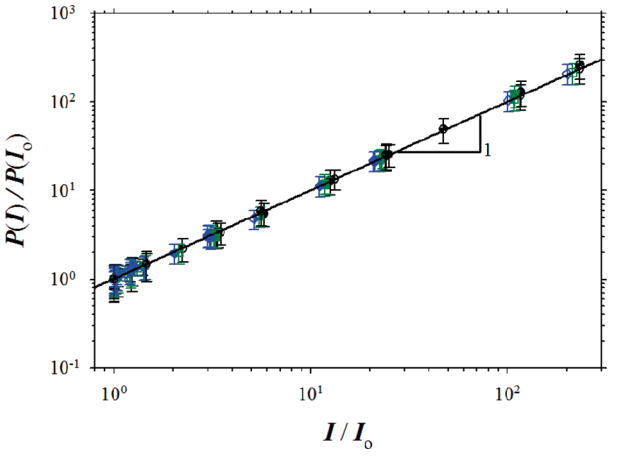

Figure 7. Dependence of the reduced pressure $P(I)/P(I_0)$ on the ratio of the ionic strengths I/I_0 for fully charged polyelectrolyte chains with the degree of polymerization $N = 300$ at polymer concentrations: $c_p = 10^{-4}\ \sigma^{-3}$ (open symbols), $c_p = 5.0 \times 10^{-4}\ \sigma^{-3}$ (half-filled symbols, hourglass), $c_p = 10^{-3}\ \sigma^{-3}$ (filled symbols), $c_p = 5.0 \times 10^{-3}\ \sigma^{-3}$ (half-filled symbols, right), $c_p = 10^{-2}\ \sigma^{-3}$ (half-filled symbols, left), and $c_p = 5.0 \times 10^{-2}\ \sigma^{-3}$ (half-filled symbols, top), and different values of the chain bending constants: $K = 0$ (black circles), $K = 3$ (green squares), and $K = 6$ (blue rhombs).

In Figure 7 we plot reduced value of the system pressure $P(I)/P(I_0)$ as a function of the ratio of the solution ionic strengths. For this plot we excluded data points corresponding to the highest polymer concentration $c_p = 0.1\ \sigma^{-3}$ and points corresponding to salt concentration $c_s = 0.05\ \sigma^{-3}$ (see discussion above).

Since the salt ions and osmotically active counterions control screening of the electrostatic interactions between charged monomers on the polymer backbone, one can expect a more general scaling relation between a quantity $X(I)$ in salt solutions and that in a salt-free solution $X(I_0)$

$$X(I) \approx X(I_0)\left(\frac{I}{I_0}\right)^{\beta} \quad (11)$$

where β is a scaling exponent. It is important to point out that in the concentration range where $f^* \approx f_0^*$ eq 11 reduces to the well-known scaling relation $X(I) \approx X(I_0)(1 + 2c_s/f^* c_p)^{\beta}$ (see for review refs 1 and 5). The invariance of the fraction of the condensed counterions, $1-f^*$, with solution ionic strength (plateau regime in Figure 6) was used for analysis of the experimental data on solution osmotic pressure,[1] solution viscosity,[1] chain's relaxation time,[1] force acting on the DNA during pore translocation,[51] and swelling of the DNA molecule in dilute solutions.[52] A new feature observed in our simulations is the decrease of the fraction of the condensed counterions at high ionic strengths. We hope that future experiments will test our observation.

The scaling relationships in dilute and semidilute polyelectrolyte solutions are discussed in details in the following sections.

5. DILUTE POLYELECTROLYTE SOLUTIONS

5.1. Chain Persistence Length. In dilute polyelectrolyte solutions the electrostatic interactions are screened at the length scales larger than the Debye screening length, r_D. The total effect of the electrostatic interactions on the chain's conformations is reduced to the local chain stiffening which is manifested in renormalization of the chain's persistence length (known as the

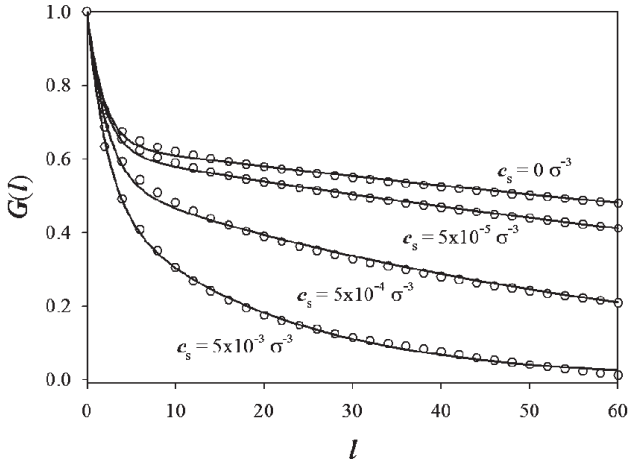

Figure 8. Bond−bond correlation function $G(l)$ for fully charged polyelectrolyte chains with the degree of polymerization $N = 300$ and chain bending constant $K = 3$ at polymer concentration $c_p = 10^{-4}\ \sigma^{-3}$ and different salt concentrations.

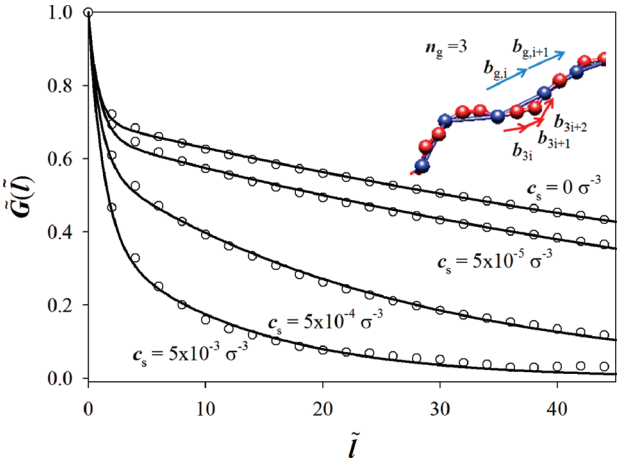

Figure 9. Bond−bond correlation function $\tilde{G}(\tilde{l})$ of coarse-grained chains with fraction of charged monomers $f = 1$, degree of polymerization $N = 300$, and chain bending constant $K = 0$ at polymer concentration $c_p = 10^{-4}\ \sigma^{-3}$ and at different salt concentrations. Inset illustrates a coarse-graining procedure for $n_g = 3$.

electrostatic persistence length[53−55]) and to the additional chain swelling which is due to interactions between remote along the polymer backbone charges.[52,55−59] We begin discussion of the effect of the salt on chain conformations in dilute polyelectrolyte solutions by analyzing orientational correlations between unit bond vectors along the polymer backbone.

The bond−bond correlation function describing decay of the orientational memory along the polymer backbone between unit bond vectors $\vec{n}_s$ and $\vec{n}_{s+l}$ pointing along the chain bonds and separated by l-bonds is defined as

$$G(l) = \frac{1}{N_b - l} \sum_{s=0}^{N_b - l - 1} \langle (\vec{n}_s \cdot \vec{n}_{s+l}) \rangle \qquad (12)$$

where N_b is the number of bonds in polyelectrolyte chain, $N_b = N - 1$, and brackets $\langle\rangle$ denote averaging over chain conformations. To minimize the end effects in obtaining the average values of the bond−bond correlation function, we have only considered 200 bonds in the middle of the chain during an averaging procedure. Figure 8 shows evolution of the bond−bond correlation function with salt concentration in dilute solution regime. To extract information about chain bending rigidity, we fitted our simulation data by combination of two exponential functions

$$G(l) = (1 - \beta_w) \exp\left(-\frac{|l|}{\lambda_1}\right) + \beta_w \exp\left(-\frac{|l|}{\lambda_2}\right) \qquad (13)$$

This form of the bond−bond correlation function indicates that there are two different characteristic length scales λ_1 and λ_2 that control bending rigidity of a polyelectrolyte chain at long and short length scales respectively (see for details ref 60). The values of the parameters λ_1 describing the chain orientational correlations at long length scales are always large such that we can expand eq 13 in the power series of l/λ_1. This results in the following modification of the eq 13

$$G(l) \approx 1 - (1 - \beta_w)\frac{|l|}{\lambda_1} + \beta_w \left(\exp\left(-\frac{|l|}{\lambda_2}\right) - 1\right) \qquad (14)$$

Note that the second term in the right-hand side of this equation has a form characteristic of a semiflexible chain under tension. We can introduce an effective chain bending constant λ_e and effective dimensionless force f_e by setting $(\lambda_e/f_e)^{1/2} = \lambda_2$ and $(\lambda_e f_e)^{1/2} = \beta_w^{-1}$. The effective chain bending rigidity at short length scales is equal to $\lambda_e = \lambda_2/\beta_w$ and the effective force is defined as $f_e = 1/\lambda_2\beta_w$. Thus, the first term in the right-hand side of eq 13 describes long-length scale bond−bond orientational correlations while the second one characterizes chain tension at short-length scales.

This approach works well for polyelectrolyte chains with bending constants $K = 3$ and 6. However, for flexible chains with $K = 0$, eq 13 fails to fit simulation data at short length scales due to fast decay of the orientational memory between bond vectors separated by several bonds. To minimize effect of the short-length scale orientational fluctuations, we applied a coarse-graining procedure by grouping original bonds and representing a chain by a set of the end-to-end vectors $\vec{b}_g$ of the bond groups consisting of n_g bonds each (see inset in Figure 9). One can think of this coarse-graining procedure as representation of the chain in terms of the electrostatic blobs and treating electrostatic blobs as new effective monomers. The optimal number of bonds n_g for this coarse- graining procedure was found self-consistently by minimizing the difference between the simulation data and eq 10. The effective bond length of the group of n_g bonds was calculated as $b_e = \langle|\vec{b}_g|\rangle$.

The results of the fitting procedure of the bond−bond correlation function are shown in Figure 10. As one can see from the plot, the value of the chain's bending constant λ_e is almost independent of the Debye screening length for polyelectrolyte chains with the bending constants equal to $K = 3$ and $K = 6$. However, it decreases with decreasing the value of the Debye screening length for chains with $K = 0$. The decrease in the effective chain bending constant λ_e is due to decrease in the number of bonds in the coarse-grained unit from 3 at low salt concentrations to 2 at high salt concentrations. The long-length scale bending constant (correlation length) λ_1 increases linearly with increasing the value of the Debye radius. For the large values of the Debye screening length the parameter λ_1 is a universal function of the Debye screening length and is independent of the initial value of the chain's bending constant K. It is important to point out that the linear scaling of the chain bending constant λ_1 on the Debye screening length is qualitatively different from a quadratic dependence observed for semiflexible

dx.doi.org/10.1021/ma2007943 |*Macromolecules* 2011, 44, 5798–5816

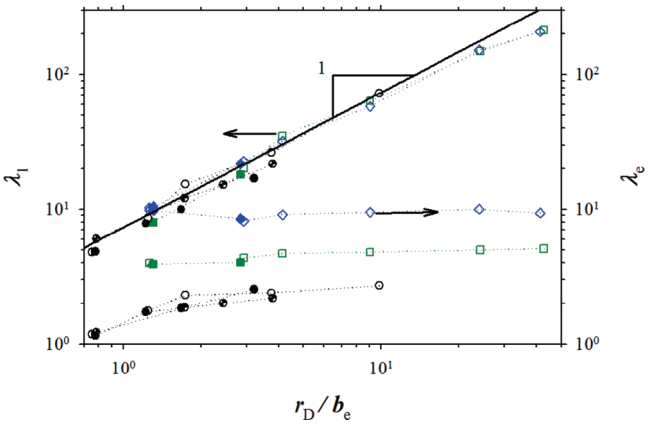

Figure 10. Dependence of the bending rigidities λ_e and λ_l on the ratio r_D/b_e (where effective bond length b_e was set to b for chains with the bending constants $K = 3$ and 6) for fully charged polyelectrolyte chains with the degree of polymerization $N = 300$ in dilute polyelectrolyte solutions at polymer concentrations: $c_p = 10^{-4}\,\sigma^{-3}$ (open symbols), $c_p = 5.0 \times 10^{-4}\,\sigma^{-3}$ (half-filled symbols, hourglass), $c_p = 10^{-3}\,\sigma^{-3}$ (filled symbols), $c_p = 5.0 \times 10^{-3}\,\sigma^{-3}$ (half-filled symbols, right), and different values of the chain bending constants: $K = 0$ (black circles), $K = 3$ (green squares), and $K = 6$ (blue rhombs).

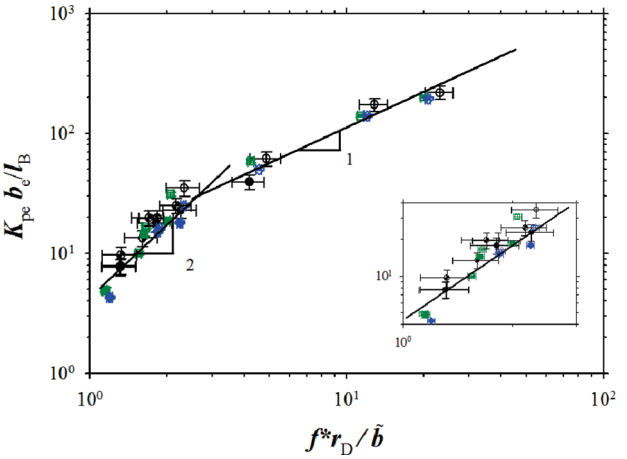

Figure 11. Dependence of the normalized value of the electrostatic bending constant $K_{pe}b_e/l_B$ on the parameter $f^*r_D/\tilde{b}$ in dilute polyelectrolyte solutions of chains with the degree of polymerization $N = 300$ at polymer concentrations: $c_p = 10^{-4}\,\sigma^{-3}$ (open symbols), $c_p = 5.0 \times 10^{-4}\,\sigma^{-3}$ (half-filled symbols, hourglass), $c_p = 10^{-3}\,\sigma^{-3}$ (filled symbols), $c_p = 5.0 \times 10^{-3}\,\sigma^{-3}$ (half-filled symbols, right), and different values of the chain bending constants: $K = 0$ (black circles), $K = 3$ (green squares), and $K = 6$ (blue rhombs).

polyelectrolyte chains interacting via the screened Debye–Huckel potential.[53–55,60–63] At low salt and polymer concentrations the data points for λ_1 begin to deviate from a straight line. This deviation is due to a finite size effect. The number of charged pairs contributing to stiffening of a chain at the length scales smaller than or on the order of the Debye screening length saturates as the Debye screening length becomes comparable with the chain size.

The linear dependence of the bending constant λ_1 is weaker than expected for the electrostatic induced chain bending rigidity. In accordance with the Odijk–Sckolnik–Fixman (OSF) theory[53,54] a chain bending constant is equal to the sum of the chain's bare bending constant K and electrostatic induced chain bending constant K_{pe}

$$\lambda_1 \approx K + K_{pe} \approx K + C\frac{l_B}{b}\left(\frac{f^* r_D}{b}\right)^2 \qquad (15)$$

where C is a numerical constant equal to 1/4 in the original OSF theory. Computer simulations of polyelectrolyte chains interacting through the screened Debye–Huckel potential show a slightly larger value of a numerical constant $C = 0.264$.[60] In the case of the coarse-grained polyelectrolyte chain consisting of coarse-grained units each having n_g bonds and effective bond length b_e, we have to substitute in eq 15 the bond length b by the effective bond length b_e, $b \to b_e$, and effective monomer valence f^* by that of the coarse grained unit f^*n_g, $f^* \to f^*n_g$. (Here and below we assume that the effective fraction of charged monomers is equal to the fraction of the osmotically active counterions. In reality, they are different by a numerical coefficient.)

It follows from eq 15 that the electrostatic contribution to the chain bending constant should demonstrate a quadratic dependence on the Debye screening length or be inversely proportional to the solution ionic strength, $\lambda_1 \propto 1/I$. However, this scaling behavior is only correct if the effective fraction of the charged monomers on the polymer backbone f^* is concentration-independent, and electrostatic interactions between charged monomers can be approximated by the Debye–Huckel potential. It follows from our Figure 6 that the fraction f^* of the osmotically active counterions increases with decreasing the Debye screening length r_D (increasing the solution ionic strength, I). This indicates that the weaker dependence of the chain bending constant λ_1 on the solution ionic strength, $\lambda_1 \propto 1/\sqrt{I}$, could be due to counterion condensation on the polymer backbone.

To test this hypothesis in Figure 11, we plot dependence of the reduced value of the electrostatic contribution to the chain bending constant $K_{pe}b_e/l_B$ as a function of the parameter $(f^*r_D/\tilde{b})$, where $\tilde{b}$ and b_e were equal to b for chains with bending constants $K = 3$ and 6, and $\tilde{b} = b_e/n_g$ for flexible chains with $K = 0$. (The parameter $(f^*r_D/\tilde{b})$ is a ratio of the Debye screening length r_D to the distance between uncompensated (osmotically active) charged monomers along the polymer backbone, $\tilde{b}/f^*$.) In Figure 11, one can clearly identify two different scaling regimes. In the range of small values of the parameter $(f^*r_D/\tilde{b})$, when the Debye screening length is only marginally larger than the distance between uncompensated charges along the polymer backbone, the reduced value of the electrostatic bending constant K_{pe} demonstrate quadratic dependence on the value of parameter $(f^*r_D/\tilde{b})$ (see eq 15). Unfortunately, the errors in the data and the covered range of parameters did not allow us to draw a definite conclusion that the observed discrepancy in Figure 11 is only due to counterion condensation. Another factor that can result in a weaker concentration dependence of the electrostatic contribution to the chain's bending constant is the nonuniform distribution of the ions around a polymer backbone. There is an excess of positive ions near the polymer backbone due to lower value of the electrostatic potential. This leads to a better screening of the polymeric charge which in turn could lead to a weaker dependence of the chain bending rigidity on the solution ionic strength. Note that in the original OSF calculations it was assumed that charges on a chain interact through a screened electrostatic (Debye–Huckel) potential. However, this approximation is only correct if polymeric charge results in a weak perturbation of the uniform ion distribution, and it breaks down in the case of strong electrostatic interactions. It is interesting to point out that the weaker than quadratic dependence of the chain

dx.doi.org/10.1021/ma2007943 |*Macromolecules* 2011, 44, 5798–5816

persistence length on the Debye screening length was also reported by Le Bret[64] and Fixman.[61] They studied contributions from nonlinear effects in ion and electrostatic potential distributions around a charged chain to a persistence length.

In the range of parameters where $(f^*r_D/\tilde{b})$ is larger than unity the reduced electrostatic bending constant, $K_{pe}b_e/l_B$, scales linearly with magnitude of the parameter $(f^*r_D/\tilde{b})$. This interval of the Debye screening lengths corresponds to low salt concentrations where screening of the polymeric charge is controlled by counterions. Also in this salt concentration regime the fraction of the condensed counterion is almost constant (see Figure 6).

In order to obtain a persistence length of a chain which orientational memory correlations are described by a bond−bond correlation function given by eq 13, we have to calculate the mean-square value of the chain end-to-end distance, $\langle \tilde{R}_e^2 \rangle$. The calculations are similar to those used for calculation of the mean-square value of the end-to-end distance of a chain with a fixed bond angle (see for details ref 45) and are reduced to summations of the geometric series. In the large N_b approximation such that both N_b/λ_1 and N_b/λ_2 are larger than unity one can show that

$$\langle \tilde{R}_e^2 \rangle \approx N_b b^2((1-\beta_w)h(\lambda_1)+\beta_w h(\lambda_2)) \qquad (16)$$

where we introduced function $h(x)$

$$h(x) = (1+\exp(-x^{-1}))/(1-\exp(-x^{-1})) \qquad (17)$$

A chain persistence length l_p is defined as

$$l_p = \frac{\langle \tilde{R}_e^2 \rangle}{2N_b b} \approx \frac{b}{2}((1-\beta_w)h(\lambda_1)+\beta_w h(\lambda_2)) \qquad (18)$$

Note that in the limit when the chain long-range bending constant $\lambda_1 \gg \lambda_2$ eq 18 can be simplified and rewritten as $l_p \approx b(1-\beta_w)\lambda_1$. In this regime the chain persistence length is determined by the value of the long-range correlation length (bending constant) λ_1.

In Figure 12, we show dependence of the chain persistence length l_p, calculated by using eq 18, on the solution ionic strength. The chain persistence length decreases with increasing the solution ionic strength as $l_p \propto 1/\sqrt{I}$. The deviation from the scaling regime occurs at low solution ionic strengths corresponding to salt-free solutions where only counterions are contributing to the screening of the polymer charge and Debye screening length becomes comparable with a chain size. Thus, in the high salt concentration regime where the screening of the electrostatic interactions is dominated by the salt ions, persistence length scales linearly with the Debye screening length. In the next section we will show how this scaling dependence of the chain persistence length manifests itself in the concentration dependence of the chain size in dilute polyelectrolyte solutions.

5.2. Chain Size. In addition to renormalization of the chain persistence length, the electrostatic interactions between charged monomers also result in chain swelling. This happens due to electrostatic repulsion between remote along the polymer backbone charged monomers. The scaling analysis of the salt effect on the polyelectrolyte chain size can be done by using a Flory-like approach by optimizing the elastic and monomer−monomer interaction contributions to the free energy of a chain with size R

$$\frac{F}{k_B T} \approx \frac{R^2}{b l_p N} + \frac{B_{el} N^2}{R^3} \qquad (19)$$

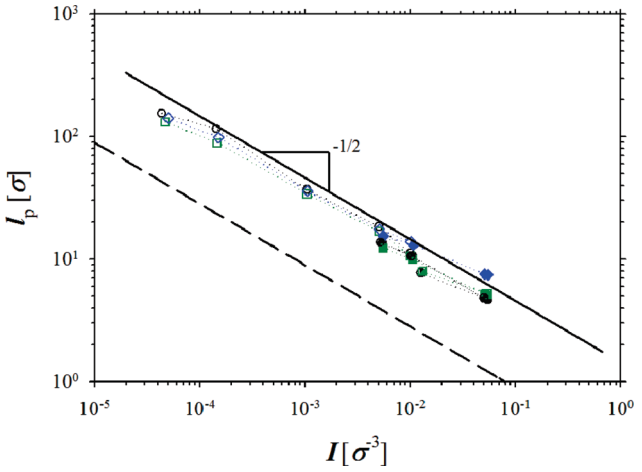

Figure 12. Dependence of the chain persistence length l_p on the solution ionic strength in dilute polyelectrolyte solutions of chains with the degree of polymerization $N = 300$ at polymer concentrations $c_p = 10^{-4}\ \sigma^{-3}$ (open symbols), $c_p = 5.0 \times 10^{-4}\ \sigma^{-3}$ (half-filled symbols, hourglass), $c_p = 10^{-3}\ \sigma^{-3}$ (filled symbols), $c_p = 5.0 \times 10^{-3}\ \sigma^{-3}$ (half-filled symbols, right), and different values of the chain bending constants $K = 0$ (black circles), $K = 3$ (green squares), and $K = 6$ (blue rhombs). Dashed line shows dependence of the Debye screening length, r_D, on the solution ionic strength.

where l_p is the chain persistence length which includes electrostatic contributions (see previous section) and B_{el} is the electrostatic second virial coefficient. In the case of the strong electrostatic interactions, when the energy of electrostatic repulsion, $U(g) \propto k_B T(l_B g^2/r_D)$ between g charges within the Debye screening length, $g \propto f^* r_D/b$, is much larger than the thermal energy $U(g) \gg k_B T$ (or $uf^{*2} > b/r_D$), the connectivity of the charged monomers into a chain plays an important role. This is manifested in appearance of the correlation hole with size on the order of the Debye screening length surrounding the polymer backbone. The electrostatic second virial coefficient between charged monomers is estimated as (see for details refs 52 and 56)

$$B_{el} \propto b^2 r_D \qquad (20)$$

Minimizing eq 19 with respect to a chain size R, we obtain

$$R \approx b(l_p r_D/b^2)^{1/5} N^{3/5} \propto N^{3/5} r_D^{2/5} \qquad (21)$$

In rewriting eq 21, we took into account the linear relationship between chain's persistence length and the Debye screening length, $l_p \propto I^{-1/2} \propto r_D$ (see Figure 12). It follows from eq 21 that the chain size decreases with solution ionic strength as $R \propto I^{-1/5}$. Figure 13 shows dependence of the mean-square value of the chain radius of gyration $\langle R_g^2 \rangle$ on the solution ionic strength. Our simulation data confirm scaling dependence $\langle R_g^2 \rangle \propto I^{-2/5}$, which is expected at high salt concentrations (see eq 21). The inset in Figure 13 shows dependence of the normalized value of the mean-square value of the chain radius of gyration on the ratio of the solution ionic strengths.

$$\frac{\langle R_g^2(I) \rangle}{\langle R_g^2(I_0) \rangle} \approx \left(\frac{I}{I_0}\right)^{-2/5} \qquad (22)$$

All data points have collapsed into one universal line confirming the validity of the scaling assumption. Note that observed dependence of the chain size on the solution ionic strength

dx.doi.org/10.1021/ma2007943 |Macromolecules 2011, 44, 5798–5816

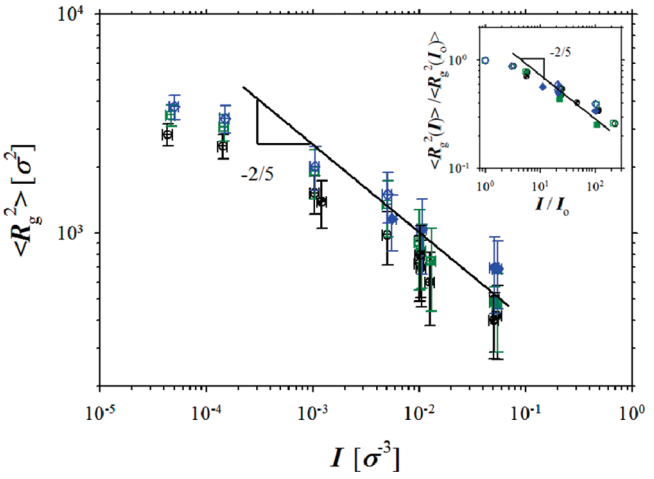

Figure 13. Dependence of the mean-square radius of gyration $\langle R_g^2 \rangle$ on the solution ionic strength in dilute polyelectrolyte solutions of chains with the degree of polymerization $N = 300$ at polymer concentrations $c_p = 10^{-4}\,\sigma^{-3}$ (open symbols), $c_p = 5.0 \times 10^{-4}\,\sigma^{-3}$ (half-filled symbols, hourglass), $c_p = 10^{-3}\,\sigma^{-3}$ (filled symbols), and different values of the chain bending constants $K = 0$ (black circles), $K = 3$ (green squares), and $K = 6$ (blue rhombs). Inset shows dependence of the reduced value of mean-square radius of gyration $\langle R_g^2(I) \rangle / \langle R_g^2(I_0) \rangle$ on the ratio of the solution ionic strengths I/I_0.

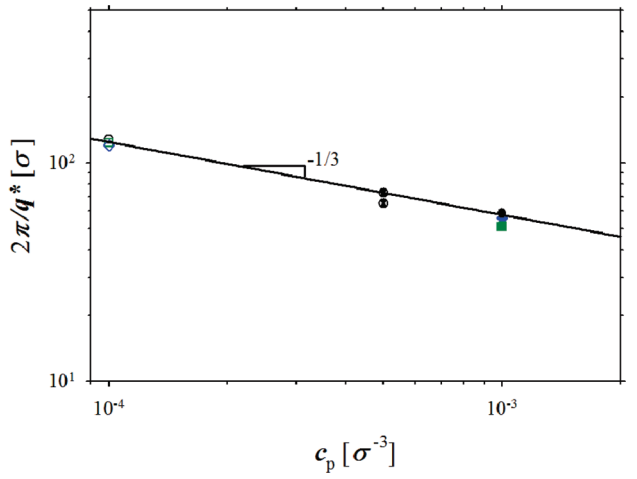

Figure 14. Dependence of $2\pi/q^*$ on polymer concentration c_p in dilute polyelectrolyte solutions of chains with the degree of polymerization $N = 300$ at polymer concentrations $c_p = 10^{-4}\,\sigma^{-3}$ (open symbols), $c_p = 5.0 \times 10^{-4}\,\sigma^{-3}$ (half-filled symbols, hourglass), $c_p = 10^{-3}\,\sigma^{-3}$ (filled symbols), and different values of the chain bending constants $K = 0$ (black circles), $K = 3$ (green squares), and $K = 6$ (blue rhombs).

$\langle R_g^2 \rangle \propto I^{-2/5}$ is weaker than one observed in simulations of polyelectrolyte chains interacting through the screened Debye–Huckel potential, $\langle R_g^2 \rangle \propto I^{-3/5}$.[55,62] The main reason for discrepancy between simulations is the counterion condensation on the polymer backbone which weakens dependence the chain persistence length on the solution ionic strength.

Using scaling relation for a chain size eq 22, we can obtain dependence of the chain overlap concentration c_p^* on the solution ionic strength. The overlap concentration c_p^* is defined as concentration at which the average concentration in a solution is equal to the monomer concentration inside polymer coil

$$c_p^* \approx \frac{N}{R(I)^3} \approx \frac{N}{R(I_0)^3}\left(\frac{I(c_p^*, c_s)}{I(c_p^*, 0)}\right)^{3/5} \tag{23}$$

At low salt concentrations ($f^* c_p \gg 2c_s$) eq 23 reduces to the expression for overlap concentration of rodlike polyelectrolyte chains ($R \propto N$) in a salt-free solution $c_p^* \propto N^{-2}$. However, at high salt concentrations ($f^* c_p \ll 2c_s$) one obtains $c_p^* \propto c_s^{3/5} N^{-4/5}$, with the same scaling dependence on the chain degree of polymerization N as in the case of neutral polymers in a good solvent for the polymer backbone.

5.3. Scattering Function and Chain Form Factor in Dilute Solutions. Information about chain structure in dilute solutions can be obtained from scattering experiments. The scattering intensity $I(\vec{q})$ at given scattering wavevector $\vec{q}$ is proportional to the scattering function $S(\vec{q})$

$$S(\vec{q}) \equiv \frac{1}{N_m} \sum_{j,k=1}^{N_m} \langle \exp(-i(\vec{q} \cdot (\vec{r}_j - \vec{r}_k))) \rangle \tag{24}$$

where $N_m = N_{ch} N$ is the total number of monomers in a system, $\vec{r}_j$ is the position of the jth monomer and brackets $\langle ... \rangle$ denote an ensemble average. In isotropic system the scattering function only depends on the magnitude of the scattering vector q. One of the characteristic features of the polyelectrolyte solutions is the presence of the peak in a scattering function (see next section and Appendix B for details). This peak appears due to suppression of the polymer density fluctuations by the requirement of the charge neutrality. In the dilute polyelectrolyte solutions the peak is located at wavenumbers $q^* \propto 1/D \propto c_p^{1/3}$ and is independent of the salt concentration (see Figure 14).[65,66,9]

At wave vectors q larger than the inverse distance between chains $1/D$ the scattering function $S(q)$ is proportional to the chain form factor $P(q)$

$$S(q) = NP(q) \tag{25}$$

where the chain form factor is defined as follows:

$$P(\vec{q}) \equiv \frac{1}{N^2} \sum_{j,k=1}^{N} \langle \exp(-i(\vec{q} \cdot (\vec{r}_j - \vec{r}_k))) \rangle$$

$$= \frac{1}{N^2} \left\langle \sum_{j,k=1}^{N} \frac{\sin(q|\vec{r}_j - \vec{r}_k|)}{q|\vec{r}_j - \vec{r}_k|} \right\rangle \tag{26}$$

The summation in eq 26 is performed over all pairs of monomers j and k, and averaging is performed over chain's configurations. At these length scales each chain is contributing independently to the total system scattering intensity. The chain form factor has the following asymptotic forms

$$P(q) \approx \begin{cases} 1 - q^2 \langle R_g^2 \rangle / 3, & \text{for } q\sqrt{\langle R_g^2 \rangle} > 1 \\ (qb)^{-d_f}, & \text{for } 1/\sqrt{\langle R_g^2 \rangle} < q < 1/b \end{cases} \tag{27a}$$

where d_f is a fractal dimension of a chain at the length scales $l \sim 1/q$. For a rodlike chain conformations $d_f = 1$.

In Figure 15a, we show evolution of the chain form factor $P(q)$ with the solution ionic strength in dilute polyelectrolyte solutions. At high q values all curves collapse, indicating that at short length scales chain are stretched with $P(q) \propto 1/q$. Experimentally, the chain form factor $P(q)$ is used to evaluate a chain persistence length[67−69] by fitting experimental data

dx.doi.org/10.1021/ma2007943 |*Macromolecules* 2011, 44, 5798–5816

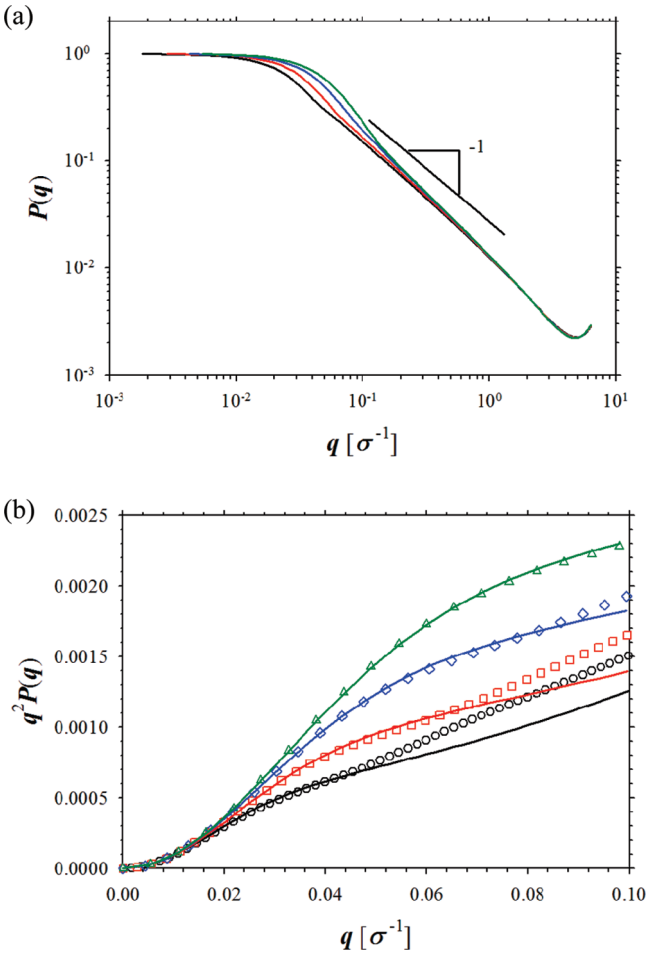

Figure 15. (a) Chain form factor $P(q)$ in dilute polyelectrolyte solutions of chains with the degree of polymerization $N = 300$ at polymer concentrations, $c_p = 10^{-4}\,\sigma^{-3}$ and salt concentrations: $c_s = 5 \times 10^{-5}\,\sigma^{-3}$ (black line), $c_s = 5 \times 10^{-4}\,\sigma^{-3}$ (red line), $c_s = 2.5 \times 10^{-3}\,\sigma^{-3}$ (blue line), and $c_s = 5 \times 10^{-3}\,\sigma^{-3}$ (green line). (b) Plot $q^2P(q)$ vs q for $c_s = 5 \times 10^{-5}\,\sigma^{-3}$ (black open circles), $c_s = 5 \times 10^{-4}\,\sigma^{-3}$ (red open squares), $c_s = 2.5 \times 10^{-3}\,\sigma^{-3}$ (blue open rhombs), and $c_s = 5 \times 10^{-3}\,\sigma^{-3}$ (green open triangle). The lines are the best fit to eq 27b considering the value of the chain persistence length l_p as a fitting parameter.

points by the function

$$P(x) = 2\frac{\exp(-x) + x - 1}{x^2} + \frac{2l_p}{bN}\left(\frac{4}{15} + \frac{7}{15x} - \left(\frac{11}{15} + \frac{7}{15x}\right)\exp(-x)\right) \tag{27b}$$

where parameter $x = q^2 b l_p N/3$. Figure 15b shows the results of the fitting procedure of the simulation data to eq 27b. The values of the fitting parameters are listed in Table 1 together with values of the persistence length evaluated from the bond−bond correlation function. As one can see from the Figure 15b, the agreement between eq 27b and simulation data is reasonably good at high salt concentrations. At low salt concentrations eq 27b completely misses the data points in the interval of large q values. Also, it follows from the Table 1 that the values of the chain persistence length obtained from the fitting procedure are always smaller than ones obtained from the analysis of the bond−bond correlation function. The main reason for the discrepancy is the assumption of the single-exponential decay of the bond−bond correlation function used for derivation of the eq 27b. As we showed in section 5.1, this assumption fails for polyelectrolyte chains for which the bond−bond correlation function is a multiscale function.

Table 1

	$c_p = 1 \times 10^{-4}\,\sigma^{-3}$	
	l_p from $G(l)$	l_p from $P(q)$ using eq 27b
$c_s = 5 \times 10^{-5}\,\sigma^{-3}$	115.3 σ	35.6 σ
$c_s = 5 \times 10^{-4}\,\sigma^{-3}$	36.8 σ	19.9 σ
$c_s = 2.5 \times 10^{-3}\,\sigma^{-3}$	18.4 σ	12.2 σ
$c_s = 5 \times 10^{-3}\,\sigma^{-3}$	11.1 σ	8.6 σ

6. SEMIDILUTE POLYELECTROLYTE SOLUTIONS

6.1. Solution Correlation Length and Scattering Function. The important length scale above the overlap concentration, $c_p > c_p^*$, is the correlation length ξ—the average mesh size of the semidilute polyelectrolyte solution.[1,5,8] It separates two different regimes in chain behavior. At the length scales smaller than the solution correlation length, the conformations of the chain sections with size smaller than the solution correlation length ξ are similar to those in dilute polyelectrolyte solutions. At the length scales larger than the solution correlation length the chain conformations are those of the random walk of the correlation blobs.

In salt free-solutions a solution correlation length can be estimated by optimizing the elastic and electrostatic parts of the chain free energy by dividing a chain into sections each containing g_ξ monomers and having size ξ

$$\frac{F}{k_B T} \propto \frac{N}{g_\xi}\left(\frac{\xi^2}{b l_p^0 g_\xi} + \frac{l_B f^{*2} g_\xi^2}{\xi}\right) \propto N\left(\frac{1}{b l_p^0 c_p{}^2 \xi^4} + l_B f^{*2} c_p \xi^2\right) \tag{28}$$

In rewriting eq 28, we took into account that the correlation blobs are space-filling, $c_p \propto g_\xi/\xi^3$, and neglected logarithmic correction to the electrostatic energy of a chain section within the correlation blob (see for details refs 1, 5, and 8). Minimizing eq 28 with respect to correlation blob size ξ, we obtain for the correlation blob size

$$\xi \approx b(uf^{*2})^{-1/6}(l_p^0/b)^{-1/6}(c_p b^3)^{-1/2} \propto c_p^{-1/2} \tag{29a}$$

and for the number of monomers per correlation blob

$$g_\xi \approx c_p \xi^3 \approx (uf^{*2})^{-1/2}(l_p^0/b)^{-1/2}(c_p b^3)^{-1/2} \propto c_p{}^{-1/2} \tag{29b}$$

where u is the ratio of the Bjerrum length l_B to bond length b, $u = l_B/b$. Comparing eqs 29a and 29b, one can conclude that the number of monomers in correlation blobs scales linearly with the blob size. Thus, chains are stretched on the length scales on the order of the solution correlation length.

In salt-solutions we can use a scaling approach to estimate correlation blob size dependence on the polymer and salt concentrations. In the framework of the scaling approach it is assumed that on the length scales on the order of the solution correlation length ξ a chain section with g_ξ monomer has the same conformation as a chain in dilute solutions at the same salt

dx.doi.org/10.1021/ma2007943 |Macromolecules 2011, 44, 5798–5816

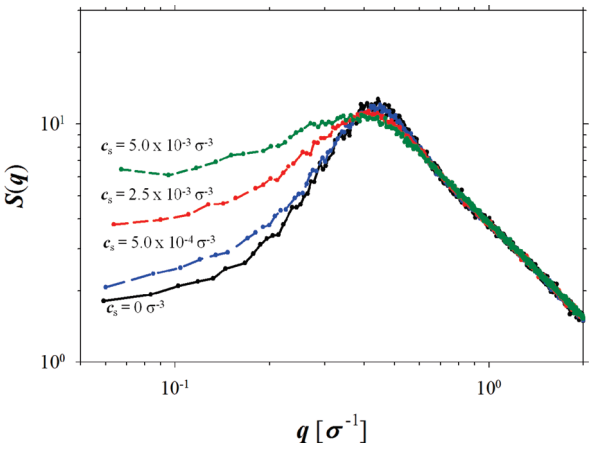

Figure 16. Scattering function $S(q)$ for fully charged polyelectrolyte chain with the degree of polymerization $N = 300$ and chain bending constant $K = 0$ at polymer concentration $c_p = 10^{-2}\,\sigma^{-3}$ and different salt concentrations.

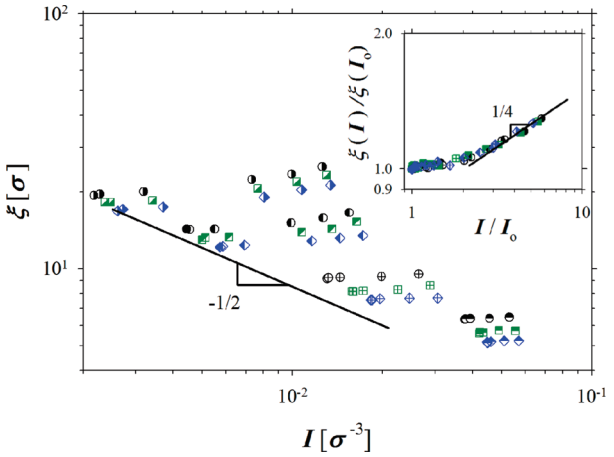

Figure 17. Dependence of the correlation length ξ on the solution ionic strength in semidilute polyelectrolyte solutions of chains with the degree of polymerization $N = 300$ at polymer concentrations $c_p = 5.0 \times 10^{-3}\,\sigma^{-3}$ (half-filled symbols, right), $c_p = 10^{-2}\,\sigma^{-3}$ (half-filled symbols, left), $c_p = 2.5 \times 10^{-2}\,\sigma^{-3}$ (open symbols, cross), $c_p = 5.0 \times 10^{-2}\,\sigma^{-3}$ (half-filled symbols, top), and different values of the chain bending constants $K = 0$ (black circles), $K = 3$ (green squares), and $K = 6$ (blue rhombs). Inset shows dependence of the reduced value of the correlation length $\xi(I)/\xi(I_0)$ on the ratio of ionic strengths I/I_0.

concentrations (see for details refs 1, 5, and 8). Taking this into account, we can write the following expression for the solution correlation length as a function of ionic strength

$$\xi(I) \approx \xi(I_0)\left(\frac{I}{I_0}\right)^{1/4} \qquad (30)$$

In low salt concentration regime ($f^* c_p \gg 2c_s$) the solution correlation length $\xi \approx \xi(I_0)$ scales with polymer concentration as $\xi \propto c_p^{-1/2}$ (see eq 29a) and is proportional to the Debye screening length. At high salt concentrations ($f^* c_p \ll 2c_s$) the concentration dependence of the solution correlation length is similar to that in solution of neutral polymers, $\xi \propto c_p^{-3/4}$. Experimentally, solution correlation length is obtained from the peak location in the scattering function $S(q)$.[65,66,69−73] As in the case of the dilute solutions, the peak appears due to suppression of the polymer density fluctuations at the length scales larger than the solution correlation length by the osmotic compressibility of the counterions and is manifestation of the electroneutrality condition (Donnan equilibrium) at these length scales. Below we used location of the peak q^* in the scattering function $S(q)$ to determined solution correlation length $\xi = 2\pi/q^*$.[8,65,66,69−72]

Note that experimental studies of polyelectrolyte solutions at low ionic strengths show an abrupt upturn in the scattering intensity at small q values.[71,74] This behavior was confirmed by neutron and light scattering studies.[71,74] Unfortunately, in our simulations we have not been able to corroborate the upturn observed in scattering experiments. Our systems are too small to separate small q upturn from the finite size effect imposed by periodic boundary conditions.

Figure 16 shows dependence of the system scattering function on the salt concentration in semidilute solution regime. It follows from this figure that with increasing the salt concentration the peak position in the scattering function shifts toward smaller values of the wavevectors. This confirms that the correlation length of the solution increases and system moves closer to the overlap concentration. At the same time the magnitude of the plateau located at small q interval increases making the peak less pronounced. Finally, at high salt concentrations the peak completely disappears. In this range of salt concentrations the scattering function has a form characteristic of that for semidilute solution of neutral polymers. The saturation of the scattering intensity occurs at $q \approx 2\pi/\xi$. Thus, we can use location of the intersection describing the crossover between two different scaling regimes in $S(q)$ dependence on the magnitude of the wavevector q for evaluation of the solution correlation length.

Figure 17 shows the dependence of the solution correlation length on the ionic strength I. All lines converge to $\xi \propto I^{-1/2}$ with increasing the solution ionic strength, which represents a scaling dependence of the solution correlation length in low salt concentration regime. In the inset to Figure 17 we test the scaling prediction eq 30 by plotting the reduced solution correlation length as a function of the reduced ionic strength. All data points have collapsed into one universal plot. However, the scaling exponent corresponding to the high salt concentration regime has a value slightly smaller than 1/4 anticipated from eq 30. We can attribute this difference to the finite size effect. With increasing the salt concentration the system moves closer to the overlap concentration, and for our chain degree of polymerizations we do not have a sufficient range of the salt concentrations to observe a pure semidilute high salt concentration regime.

The change of the chain conformations on the length scales on the order of the solution correlation length can be monitored by plotting dependence of the correlation length ξ on the number of monomers g_ξ within correlation length. In order to obtain g_ξ, we used dependence of the square root of the mean-square value of the end-to-end distance $\langle R_e^2(n)\rangle^{1/2}$ of a section of a chain consisting of n monomers. The results are shown in Figure 18. At low salt concentrations and salt-free solution regime there is a linear relationship between the solution correlation length ξ and the number of monomers within the correlation length g_ξ. The linear relationship between $\xi \propto g_\xi$ confirms the scaling assumption that the chain is stretched on the length scales smaller than the solution correlation length (see eqs 29a and 29b). With increasing salt concentration the number of monomers g_ξ within correlation length increases. This increase is accompanied by the change in power law dependence of ξ as a function of g_ξ. In this salt concentration regime the data points approach a scaling law

dx.doi.org/10.1021/ma2007943 |*Macromolecules* 2011, 44, 5798–5816

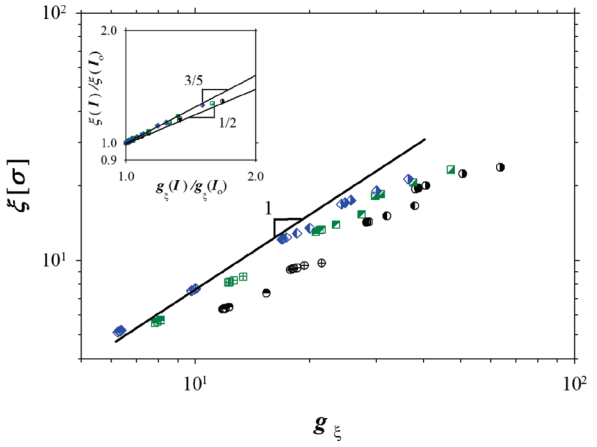

Figure 18. Dependence of the correlation length ξ on the number of monomers within the correlation length g_ξ in semidilute polyelectrolyte solutions of chains with the degree of polymerization $N = 300$ at polymer concentrations $c_p = 5.0 \times 10^{-3}\,\sigma^{-3}$ (half-filled symbols, right), $c_p = 10^{-2}\,\sigma^{-3}$ (half-filled symbols, left), $c_p = 2.5 \times 10^{-2}\,\sigma^{-3}$ (open symbols, cross), $c_p = 5.0 \times 10^{-2}\,\sigma^{-3}$ (half-filled symbols, top), and different values of the chain bending constants $K = 0$ (black circles), $K = 3$ (green squares), and $K = 6$ (blue rhombs). Inset shows dependence of the reduced value of the correlation length $\xi(I)/\xi(I_0)$ on the reduced number of monomers within the correlation length $g_\xi(I)/g_\xi(I_0)$.

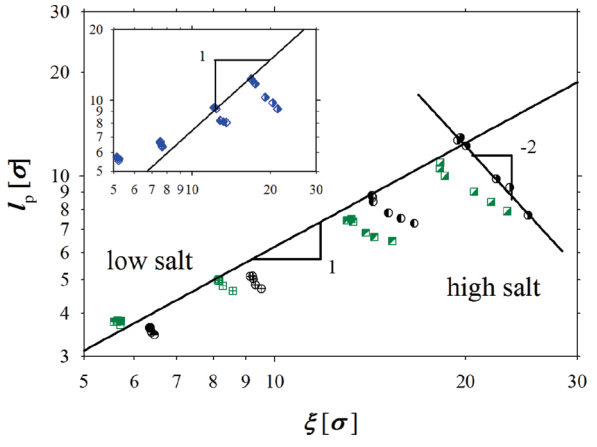

Figure 19. Dependence of the chain persistence length l_p on correlation length ξ in semidilute polyelectrolyte solutions of chains with the degree of polymerization $N = 300$ at polymer concentrations $c_p = 5.0 \times 10^{-3}\,\sigma^{-3}$ (half-filled symbols, right), $c_p = 10^{-2}\,\sigma^{-3}$ (half-filled symbols, left), $c_p = 2.5 \times 10^{-2}\,\sigma^{-3}$ (open symbols, cross), $c_p = 5.0 \times 10^{-2}\,\sigma^{-3}$ (half-filled symbols, top), and different values of the chain bending constants $K = 0$ (black circles), $K = 3$ (green squares), and $K = 6$ (blue rhombs).

$\xi \propto g_\xi^{\nu}$ with exponent ν between 3/5 and 1/2 (see inset in Figure 18). Unfortunately, the sections of a chain within correlation length ξ are too short to distinguish between 3/5 and 1/2 exponents.

6.2. Chain Persistence Length. The chain persistence length in semidilute solution regime was obtained from fitting a chain bond−bond correlation function (see eq 12) by sum of two exponentials (see eq 13) and using relation eq 18 between fitting parameters and chain persistence length. The results of this procedure are summarized in Figure 19. At low salt concentrations, $f^*c_p > 2c_s$, when the screening of the electrostatic interactions is dominated by counterions, the chain persistence length is proportional to the

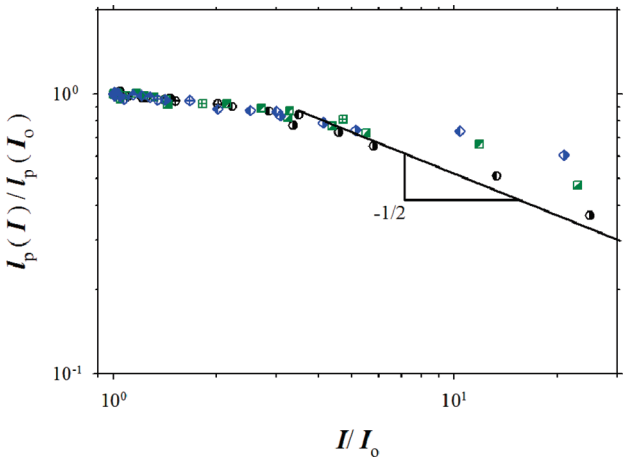

Figure 20. Dependence of the reduced chain persistence length $l_p(I)/l_p(I_0)$ on the ratio of the solution ionic strengths I/I_0 in semidilute polyelectrolyte solutions of chains with the degree of polymerization $N = 300$ at polymer concentrations $c_p = 5.0 \times 10^{-3}\,\sigma^{-3}$ (half-filled symbols, right), $c_p = 10^{-2}\,\sigma^{-3}$ (half-filled symbols, left), $c_p = 2.5 \times 10^{-2}\,\sigma^{-3}$ (open symbols, cross), $c_p = 5.0 \times 10^{-2}\,\sigma^{-3}$ (half-filled symbols, top), and different values of the chain bending constants $K = 0$ (black circles), $K = 3$ (green squares), and $K = 6$ (blue rhombs).

solution correlation length, $l_p \propto \xi \propto c_p^{-1/2}$.[1,5,75] In this salt concentration interval the bending of the polyelectrolyte chain is caused by repulsion from neighboring chains because the Debye screening length due to free counterions and salt ions is larger than the solution correlation length ξ. It is also important to point out that in this salt concentration regime the sections of the chain are also contributing to the screening of the electrostatic interactions setting up the electrostatic screening length to be on the order of the solution correlation length. For detailed discussion of the screening effects in semidilute polyelectrolyte solutions see refs 1 and 5. The deviation from the linear relationship between persistence length and correlation length occurs at high polymer concentrations when correlation length becomes comparable with the bare chain persistence length of a chain l_p^0. This can be clearly seen in the inset in Figure 19 which shows data for polyelectrolyte chains with the bending constant $K = 6$.

At high salt concentrations, $f^*c_p < 2c_s$, the chain persistence length decreases with increasing solution correlation length ξ. In this range of salt and polymer concentrations the persistence length is inversely proportional to the square of the solution correlation length, $l_p \propto \xi^{-2}$. Taking into account the scaling relation between correlation length ξ and ionic strength I, $\xi \propto I^{1/4}$ (see eq 30), one can show that the chain persistence length l_p is inversely proportional to the square root of the solution ionic strength I. Thus, in this high salt concentration regime we see the same salt concentration dependence of the chain persistence length as in dilute polyelectrolyte solutions (see Figure 12). In Figure 20, we plot $l_p(I)/l_p(I_0)$ as a function of the ratio of the solution ionic strengths. The data sets group into three groups according to the values of the bare chain persistence length. For systems with $K = 0$ and $K = 3$ the high salt data sets approach a scaling law

$$l_p(I) \approx l_p(I_0)\left(\frac{I}{I_0}\right)^{-1/2} \qquad (31)$$

6.3. Chain Size Scaling. The scaling model of a polyelectrolyte chain in semidilute solutions is based on the assumption

dx.doi.org/10.1021/ma2007943 |*Macromolecules* 2011, 44, 5798–5816

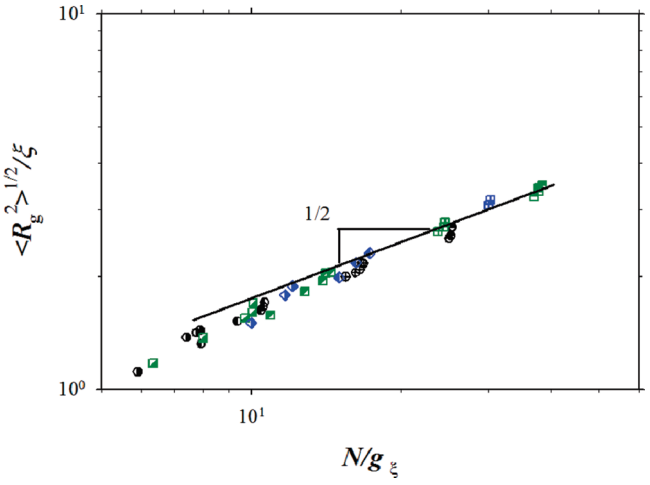

Figure 21. Dependence of the ratio of the square root of the mean-square radius of gyration and correlation length $\langle R_g^2\rangle^{1/2}/\xi$ on the ratio of the degree of polymerization N and the number of monomers within the correlation length g_ξ in semidilute polyelectrolyte solutions of chains with the degree of polymerization $N = 300$ at polymer concentrations $c_p = 5.0 \times 10^{-3}\,\sigma^{-3}$ (half-filled symbols, right), $c_p = 10^{-2}\,\sigma^{-3}$ (half-filled symbols, left), $c_p = 2.5 \times 10^{-2}\,\sigma^{-3}$ (open symbols, cross), $c_p = 5.0 \times 10^{-2}\,\sigma^{-3}$ (half-filled symbols, top), and different values of the chain bending constants $K = 0$ (black circles), $K = 3$ (green squares), and $K = 6$ (blue rhombs).

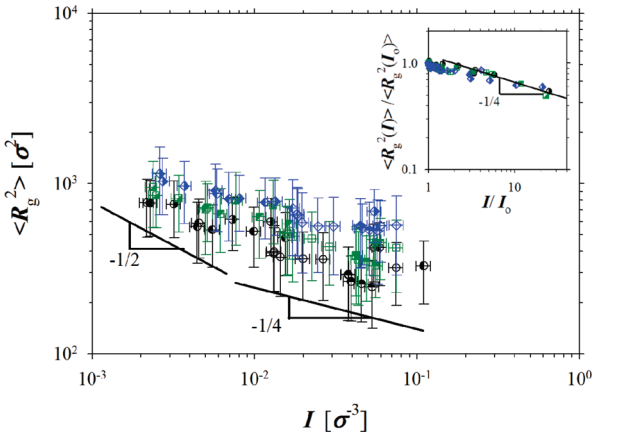

Figure 22. Dependence of the mean-square radius of gyration $\langle R_g^2\rangle$ on the solution ionic strength in semidilute polyelectrolyte solutions of chains with the degree of polymerization $N = 300$ at polymer concentrations $c_p = 5.0 \times 10^{-3}\,\sigma^{-3}$ (half-filled symbols, right), $c_p = 10^{-2}\,\sigma^{-3}$ (half-filled symbols, left), $c_p = 2.5 \times 10^{-2}\,\sigma^{-3}$ (open symbols, cross), $c_p = 5.0 \times 10^{-2}\,\sigma^{-3}$ (half-filled symbols, top), and different values of the chain bending constants $K = 0$ (black circles), $K = 3$ (green squares), and $K = 6$ (blue rhombs). Inset shows dependence of the reduced value of mean-square radius of gyration $\langle R_g^2(I)\rangle/\langle R_g^2(I_0)\rangle$ on the ratio of the solution ionic strengths I/I_0.

of the existence of a single length scale—the correlation length ξ.[1,5,8] At the length scales larger than the solution correlation length ξ, other chains and counterions screen electrostatic interactions, and the statistics of the chain are those of a Gaussian chain with the effective persistence length on the order of the correlation length ξ. Thus, the polyelectrolyte chain is assumed to be flexible at the length scales on the order of the correlation length ξ. According to the scaling model, a chain in the semidilute polyelectrolyte solution is a random walk of correlation blobs with size

$$R \approx \xi\left(\frac{N}{g_\xi}\right)^{1/2} \tag{32}$$

To test scaling hypothesis for the chain size dependence on the number of correlation blobs per chain, the plot of the normalized chain size $(\langle R_g^2\rangle)^{1/2}/\xi$ as a function of the number of correlation blobs per chain N/g_ξ is shown in Figure 21. All points for chains at different polymer and salt concentrations collapse onto one universal line, with the slope 1/2 as expected for Gaussian chains with N/g_ξ correlation blobs. There is a slight deviation from universal behavior in the range of small number of the correlation blobs per chain.

Using expression for the chain size dependence on the number of blobs per chain and solution correlation length ξ, we can derive expression for the chain size as a function of the solution ionic strength. For a mean-square value of the chain radius of gyration we have

$$\langle R_g^2(I)\rangle \approx \xi(I)^2\frac{N}{g_\xi(I)} \approx \langle R_g^2(I_0)\rangle\frac{\xi(I_0)}{\xi(I)} \tag{33}$$

In rewriting the last equation, we took into account that the correlation blobs are space-filling and $c_p \approx g_\xi(I)/\xi(I)^3 \approx g_\xi(I_0)/\xi(I_0)^3$. Using eq 30, we can express the ratio of the solution correlation lengths in terms of the ratio of ionic strengths. This results in the following expression for a mean-square value of the chain radius of gyration

$$\langle R_g^2(I)\rangle \approx \langle R_g^2(I_0)\rangle\left(\frac{I}{I_0}\right)^{-1/4} \tag{34}$$

In low salt concentration regime eq 33 reduces to $\langle R_g^2\rangle \propto N^{1/2}c_p^{-1/2}$, while at high salt concentration limit the chain size scales with polymer concentration as $\langle R_g^2\rangle \propto N^{1/2}c_p^{-1/4}$ recovering the polymer concentration of the chain size in solutions of neutral polymers.[1,5] Figure 22 combines our simulation data for dependence of the mean-square value of the chain radius of gyration in semidilute solution regime. As expected at low salt concentration limit the data follow $\langle R_g^2\rangle \propto I^{-1/2}$ scaling dependence while at high salt concentrations we see $\langle R_g^2\rangle \propto I^{-1/4}$. To collapse all our simulation data into one universal plot in the inset, we plot the ratio of the mean-square value of the chain radius of gyration $\langle R_g^2(I)\rangle$in salt solutions to that in a salt-free solution as a function of the ratio of the solution ionic strengths (see eq 34). Data collapse into one universal line with slope −1/4, thus confirming eq 34.

7. SUMMARY

We performed molecular dynamics simulations of salt solutions of polyelectrolyte chains with the degree of polymerization $N = 300$. Polyelectrolyte chains were modeled by Lennard-Jones particles connected by the finite extension nonlinear elastic bonds. The mutual orientation of the neighboring along the polymer backbone bonds was maintained by imposing an angular potential. The counterions and salt ions were included explicitly into our simulations.

Our simulations show that in salt-free solutions in polymer concentration range $c_p \geq 10^{-4}\,\sigma^{-3}$ osmotic coefficient show a plateau then increases with increasing polymer concentration. At polymer concentrations c_p larger than $5 \times 10^{-2}\,\sigma^{-3}$ the value of the osmotic coefficient exceeds unity, indicating that polymeric and excluded volume effects begin to contribute to the system pressure. For lower polymer concentrations we related the value

dx.doi.org/10.1021/ma2007943 |Macromolecules 2011, 44, 5798–5816

Table 2. Scaling Relations for Dilute and Semidilute Polyelectrolyte Solutions

	dilute solutions	semidilute solutions
$P(I)$	$P(I_0)I/I_0$	$P(I_0)I/I_0$
$\langle R_g^2(I)\rangle$	$\langle R_g^2(I_0)\rangle(I/I_0)^{-2/5}$	$\langle R_g^2(I_0)\rangle(I/I_0)^{-1/4}$
$\xi(I)$		$\xi(I_0)(I/I_0)^{1/4}$
$l_p(I)$	$l_p(I_0)(I/I_0)^{-1/2}$	$l_p(I_0)(I/I_0)^{-1/2}$

of the osmotic coefficient with the fraction of osmotically active counterions. In the salt solutions the fraction of osmotically active counterions was obtained from the difference between system pressure P and ideal pressure of salt ions, $2k_BTc_s$ (see eq 6). The fraction of osmotically active counterions f^* shows a weak dependence on the chain bending rigidity, K. It has a smaller value for flexible chains with bending constant $K = 0$ and increases with increasing the chain's bending rigidity (see Figure 6). This is manifestation of the crumpling of a chain at short length scales and higher linear charge density for chains with $K = 0$ in comparison with that for more rigid chains. Using fraction of osmotically active counterions f^* obtained from counterion contribution to the system pressure, we defined ionic strength of the solution I (see eq 10) and verified a general scaling relation between a quantity $X(I)$ in salt solutions and that in a salt-free solution $X(I_0)$. The results are summarized in Table 2.

In dilute and semidilute solution regimes the electrostatic interactions between charged monomers result in chain stiffening. Our analysis of the bond−bond correlation function shows that chain persistence length l_p is inversely proportional to the square root of the solution ionic strength, $l_p \propto 1/\sqrt{I}$. This dependence of the chain persistence length is weaker than predicted by the OSF model,[53−55,60,61] $l_p^{OSF} \propto I^{-1}$, and observed in computer simulations of the polyelectrolyte chains interacting via screened Coulomb potential.[60,62,63] We showed that the weaker dependence of the chain persistence length on the solution ionic strength can be explained by counterion condensation on the polymer backbone. The square root dependence of the chain persistence length on the solution ionic strength in dilute solution regime is in agreement with a chain size R decrease with ionic strength as $R \propto I^{-1/5}$ (see Figure 13).

The correlation length ξ is an important length scale in semidilute solution regime, which separates two different length scales. At the length scales smaller than the solution correlation length the chain statistics is the same as in a dilute solution while at the length scales larger than the solution correlation length the interactions between monomers are screened and chain behaves as a Gaussian chain of correlation blobs. The value of the solution correlation length was obtained from the peak position in the polymer scattering function $S(q)$. At low salt concentrations we observed the exponent for the concentration dependence of the solution correlation length to be close to $c_p^{-1/2}$, in agreement with the scaling model of semidilute polyelectrolyte solutions. In the high salt concentration regime, $f^*c_p < 2c_s$, our data confirm a general scaling relation $\xi(I) \approx \xi(I_0)(I/I_0)^{1/4}$ (see Figure 17). This dependence of the solution correlation length is in agreement with the scaling of the chain persistence length with ionic strength as $l_p \propto I^{-1/2}$. We have also tested a scaling assumption that in salt-free solutions the chain persistence length is proportional to the solution correlation length (see Figure 19). This was further corroborated by the scaling of the reduced chain size R/ξ on the number of correlation blobs per chain N/g_ξ (see Figure 21). Thus, in salt-free solutions in semidilute solution regime a polyelectrolyte chain can be considered as a random walk of correlation blobs. Note that in this salt concentration range the number of monomers within correlation length scales linearly with its size. At high salt concentrations the chain size R decreases with increasing the solution ionic strength as $R \propto I^{-1/8}$ (see Figure 22). This scaling relation provides additional evidence for inverse square root dependence of the chain persistence length on the solution ionic strength, $l_p \propto I^{-1/2}$.

In our study of the effect of the salt on the polyelectrolyte solution properties we only considered the effect of monovalent ions. The behavior of polyelectrolytes in the presence of divalent ions is qualitatively different from that in solutions of monovalent salts.[76−81] In the case of divalent ions the counterion condensation on the polymer backbone can lead to chain associations and phase separation.[78,79,81] We are planning to consider these effects in a separate publication.

APPENDIX A. SIMULATION DETAILS

We performed molecular dynamics simulations of polyelectrolyte chains with explicit counterions and salt ions. Polyelectrolytes were modeled by chains of charged Lennard-Jones (LJ) particles (beads) with diameter σ and degree of polymerization $N = 300$. Each monomer on the polymer backbone was charged. Counterions and salt ions were modeled as LJ particles (beads) with diameter σ. The solvent was treated implicitly as a dielectric medium with dielectric constant ε.

All particles in the system interacted through truncated-shifted Lennard-Jones (LJ) potential:

$$U_{LJ}(r_{ij}) = \begin{cases} 4\varepsilon_{LJ}\left[\left(\frac{\sigma}{r_{ij}}\right)^{12} - \left(\frac{\sigma}{r_{ij}}\right)^{6} - \left(\frac{\sigma}{r_{cut}}\right)^{12} + \left(\frac{\sigma}{r_{cut}}\right)^{6}\right] & r \le r_{cut} \\ 0 & r > r_{cut} \end{cases} \quad (A.1)$$

where r_{ij} is the distance between ith and jth beads and σ is the bead diameter chosen to be the same regardless of the bead type. The cutoff distance, $r_{cut} = 2.5\sigma$, was set for polymer−polymer interactions, and $r_{cut} = 2^{1/6}\sigma$ was selected for all other pairwise interactions. The interaction parameter ε_{LJ} was equal to k_BT for polymer−ion and ion−ion interactions. The value of the Lennard-Jones interaction parameter for the polymer−polymer pairs was set to $0.3k_BT$, which is close to a theta solvent condition for the polymer backbone. By selecting the strength of the polymer−polymer interactions close to the θ-point, we minimized the effect of the short-range interactions on polyelectrolyte solution properties.

The connectivity of monomers into polymer chains was maintained by the finite extension nonlinear elastic (FENE) potential:

$$U_{FENE}(r) = -\frac{1}{2}k_{spring}R_{max}^2 \ln\left(1 - \frac{r^2}{R_{max}^2}\right) \quad (A.2)$$

with the spring constant $k_{spring} = 30k_BT/\sigma^2$ and the maximum bond length $R_{max} = 1.2\sigma$. The repulsive part of the bond potential was represented by the truncated-shifted LJ potentials with $\varepsilon_{LJ} = 1.5k_BT$ and $r_{cut} = 2^{1/6}\sigma$.

The chain bending rigidity was introduced into the model through a bending potential controlling the mutual orientations between two neighboring along the polymer backbone unit bond

dx.doi.org/10.1021/ma2007943 |Macromolecules 2011, 44, 5798–5816

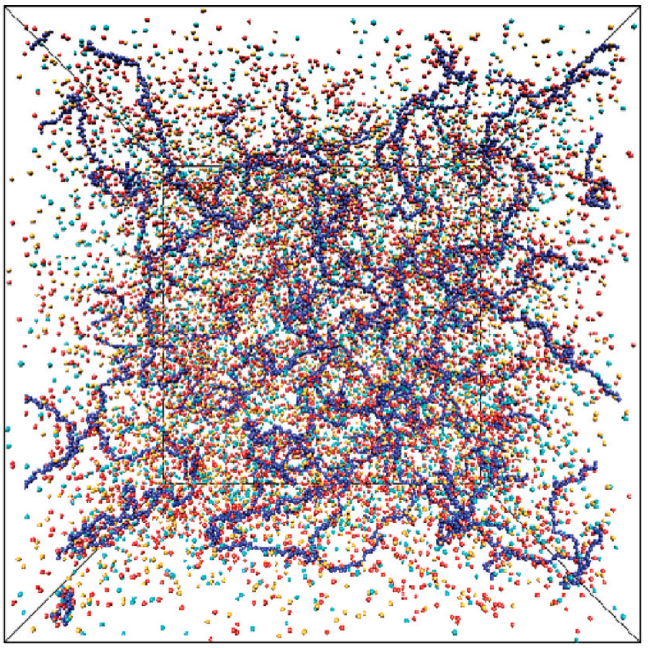

Figure 23. Snapshot of the simulation box containing fully charged polyelectrolyte chains, counterions, and salt ions. The polyelectrolyte chains are shown in blue, chain counterions are shown in red, and cyan and orange colored beads represent negatively and positively charged salt ions, respectively.

vectors $\vec{n}_i$ and $\vec{n}_{i+1}$

$$U_{i,i+1}^{\text{bend}} = k_B TK(1 - (\vec{n}_i \cdot \vec{n}_{i+1})) \quad (A.3)$$

The bending constant K was equal to 0, 3, and 6.

Interaction between any two charged particles with charge valences q_i and q_j, and separated by a distance r_{ij}, was given by the Coulomb potential

$$U_{\text{Coul}}(r_{ij}) = k_B T \frac{l_B q_i q_j}{r_{ij}} \quad (A.4)$$

where $l_B = e^2/\varepsilon k_B T$ is the Bjerrum length. In our simulations, the value of the Bjerrum length l_B was equal to 1.0σ. The particle−particle particle−mesh (PPPM) method implemented in LAMMPS[82] with the sixth-order charge interpolation scheme and estimated accuracy 10^{-5} was used for calculations of the electrostatic interactions between all charges in the system.

Simulations were carried out in a constant number of particles, volume, and temperature ensemble (NVT) with periodic boundary conditions. The snapshot of the simulation box is shown in Figure 23. The simulation box sizes, number of particles in simulation box, and covered polymer and salt concentrations are summarized in Table 3.

The simulations were performed at a constant temperature, which was maintained by coupling the system to the Langevin thermostat. The motion of beads was described by the following equation

$$m\frac{d\vec{v}_i(t)}{dt} = \vec{F}_i(t) - \xi\vec{v}_i(t) + \vec{F}_i^R(t) \quad (A.5)$$

where m is the bead mass, $\vec{v}_i(t)$ is the bead velocity, and $\vec{F}_i(t)$ denotes the net deterministic force acting on the ith bead. The stochastic force $\vec{F}_i^R(t)$ has a zero average value $\langle\vec{F}_i^R(t)\rangle = 0$ and

Table 3. List of Studied Systems

c_p [σ^{-3}]	c_s [σ^{-3}]	L_x [σ]	N_{ch}	N_{cion}	N_{salt}	N_{total}
0.0	0.00005	368.40	0	0	5000	5000
	0.0005	171.00	0	0	5000	5000
	0.0025	100.00	0	0	5000	5000
	0.005	79.37	0	0	5000	5000
	0.025	46.42	0	0	5000	5000
	0.05	36.84	0	0	5000	5000
0.0001	0	493.24	40	12000	0	24000
	0.00005	432.68	27	8100	8100	24300
	0.0005	275.89	7	2100	21000	25200
	0.0025	181.71	2	600	30000	31200
	0.005	144.23	1	300	30000	30600
0.0005	0	288.45	40	12000	0	24000
	0.00005	278.50	36	10800	2160	23760
	0.0005	228.94	20	6000	12000	24000
	0.0025	161.34	7	2100	21000	25200
	0.005	133.89	4	1200	24000	26400
	0.025	84.34	1	300	30000	30600
0.001	0	228.94	40	12000	0	24000
	0.00005	225.06	38	11400	1140	23940
	0.0005	200.83	27	8100	8100	24300
	0.0025	148.88	11	3300	16500	23100
	0.005	128.06	7	2100	21000	25200
	0.025	84.34	2	600	30000	31200
	0.05	66.94	1	300	30000	30600
0.005	0	133.89	40	12000	0	24000
	0.00005	133.89	40	12000	240	24240
	0.0005	129.27	36	10800	2160	23760
	0.0025	117.45	27	8100	8100	24300
	0.005	106.27	20	6000	12000	24000
	0.025	74.89	7	2100	21000	25200
	0.05	62.14	4	1200	24000	26400
0.01	0	106.27	40	12000	0	24000
	0.00005	106.27	40	12000	120	24120
	0.0005	104.46	38	11400	1140	23940
	0.0025	106.27	40	12000	6000	30000
	0.005	106.27	40	12000	12000	36000
	0.025	106.27	40	12000	60000	84000
	0.05	59.44	7	2100	21000	25200
0.025	0	78.30	40	12000	0	24000
	0.00005	78.30	40	12000	48	24048
	0.0005	77.64	39	11700	468	23868
	0.0025	75.60	36	10800	2160	23760
	0.005	73.43	33	9900	3960	23760
	0.025	62.14	20	6000	12000	24000
0.05	0	62.14	40	12000	0	24000
	0.00005	62.14	40	12000	24	24024
	0.0005	62.14	40	12000	240	24240
	0.0025	61.09	38	11400	1140	23940
	0.005	60.00	36	10800	2160	23760
	0.025	54.51	27	8100	8100	24300
	0.05	49.32	20	6000	12000	24000
0.1	0	49.32	40	12000	0	24000
	0.00005	49.32	40	12000	12	24012
	0.0005	49.32	40	12000	120	24120
	0.0025	48.91	39	11700	585	23985
	0.005	48.49	38	11400	1140	23940
	0.025	45.79	32	9600	4800	24000
	0.05	43.27	27	8100	8100	24300

dx.doi.org/10.1021/ma2007943 |*Macromolecules* 2011, 44, 5798–5816

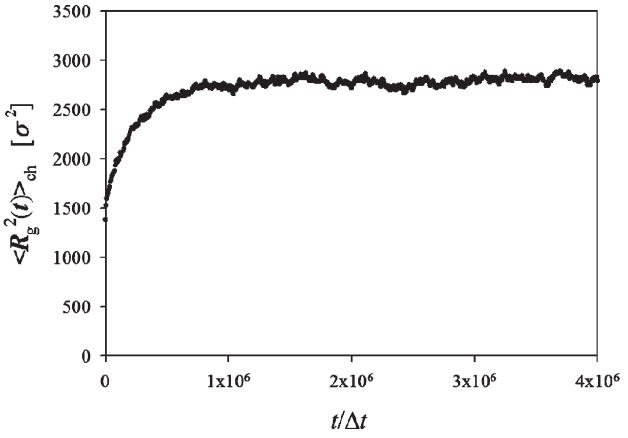

Figure 24. Evolution of the mean-square value of the radius of gyration during simulation run in salt-free solution of fully charged polyelectrolyte chains with the degree of polymerization $N = 300$, chain bending constant $K = 0$, at polymer concentration $c_p = 1 \times 10^{-4}\ \sigma^{-3}$.

δ-functional correlations $\langle \vec{F}_i^R(t)\vec{F}_i^R(t')\rangle = 6k_BT\xi\delta(t - t')$. The friction coefficient ξ was set to $\xi = 0.143m/\tau_{LJ}$, where τ_{LJ} is the standard LJ time $\tau_{LJ} = \sigma(m/k_BT)^{1/2}$. The velocity-Verlet algorithm with a time step $\Delta t = 0.01\tau_{LJ}$ was used for integration of the equations of motion eq A.5. All simulations were performed using LAMMPS.[82]

Simulations were performed using the following procedure: at the beginning of each simulation run polyelectrolyte chains in the self-avoiding walk conformation, counterions and salt ions were randomly distributed over the volume of the simulation box. This followed by the equilibration step. The equilibration step continued until the mean-square value of the chain radius of gyration averaged over all chains in the simulation box reached saturation. This followed by a production run lasting 2×10^6 integration steps. Figure 24 shows evolution of the mean-square average value of the radius of gyration. At each time step the average was calculated over all chains in a system. Note that the total duration of the simulation runs was varied between 4×10^6 and 8×10^6 integration steps, depending on how long it took for the system to reach equilibrium.

Let us relate the parameters used in our coarse-grained MD simulations of polyelectrolyte solutions with charged polymeric systems. In the bead−spring representation of a polymer chain, each bead represents several chemical units. For example, if we assume that the value of the Bjerrum length, $l_B = 1\sigma$, used in our simulations is equal to the Bjerrum length in water at room temperature ($T = 298$ K), $l_B = 0.714$ nm, the monomer size is equal to 0.714 nm. This corresponds approximately to 2.9 monomers of sodium poly(styrenesulfonate) with monomer size 0.25 nm and leads to a polymer chain with the degree of polymerization on the order of 870 monomers. The polymer concentrations in our simulations correspond to polyelectrolyte solutions with polymer concentrations $4.6 \times 10^{-4} \le c_p \le 4.6 \times 10^{-1}$ M. The salt concentrations used in our simulations correspond to salt concentrations of NaCl within the range $2.3 \times 10^{-4} \le c_s \le 2.3 \times 10^{-1}$ M.

■ APPENDIX B. CALCULATIONS OF THE SCATTERING FUNCTION

Scattering function $S(\vec{q})$ provides information about conformations of polyelectrolyte chains and structural properties of the solution. It is defined as

$$S(\vec{q}) = \frac{1}{N_m}\left\langle \sum_{k,j}^{N_m} \exp(i(\vec{q}\cdot(\vec{r}_k - \vec{r}_j)))\right\rangle \qquad (B.1)$$

The summation in eq B.1 is taken over all pairs of monomers $N_m = N_{ch}N$ in a system, $\vec{r}_k$ is the radius vector of the kth monomer, and brackets $\langle ... \rangle$ denote the ensemble average. In performing calculations of the eq B.1, it is useful to introduce a Fourier transform of the monomer density in a given system configuration

$$\rho(\vec{q}) = \sum_{k=1}^{N_m} \exp(i(\vec{q}\cdot\vec{r}_k)) \qquad (B.2)$$

In terms of the $\rho(\vec{q})$ the scattering function can be rewritten as

$$S(\vec{q}) = \frac{1}{N_m}\langle \rho(\vec{q})\rho(-\vec{q})\rangle \qquad (B.3)$$

Thus, calculation of the scattering function is reduced to calculation of the $\rho(\vec{q})$ in a given system configuration. The FFT is an efficient method in calculating of the Fourier transform of the special distributed function. To apply an FFT method to our system, we represented the actual monomer distribution by distribution over $N_g = L/\Delta$ grid points. The number of the grid points was varied between 128 and 256 depending on the system sizes. The distance between the grid points was selected from the interval $b/2 \le \Delta < b$ to satisfy the condition that the number of the grid points was a power of 2. We used a linear interpolation scheme to smear a monomer between neighboring grid points. In this representation the function $\rho(\vec{q})$ was transformed to

$$\rho(\vec{q}) = \rho(l,m,n) = \sum_{s,j,h=0}^{N_g-1} \exp\left(i\frac{2\pi}{N_g}(ls + mj + nh)\right) n(s,j,h) \qquad (B.4)$$

where $n(s,j,h)$ is a number of monomers in a grid point with coordinates s, j, and h. Note that wavevector $\vec{q}$ has coordinates $q_x = 2\pi l/L$, $q_y = 2\pi m/L$, $q_z = 2\pi n/L$, and $q = (q_x^2 + q_y^2 + q_z^2)^{1/2}$. The FFT method was used to calculate the complex function $\rho(l,m,n)$. Knowing function $\rho(l,m,n)$, we have calculated the scattering function in grid points

$$S(l,m,n) = \frac{1}{N_m}\langle (\mathrm{Re}\ \rho(l,m,n))^2 + (\mathrm{Im}\ \rho(l,m,n))^2\rangle \qquad (B.5)$$

where Re $\rho(l,m,n)$ and Im $\rho(l,m,n)$ are real and imaginary parts of the complex number $\rho(l,m,n)$. Figure 25 shows results of the 3-D FFT of the polyelectrolyte system.

For isotropic systems one can use a 1-D FFT by pointing vector $\vec{q}$ along x-axis, $q = q_x$. Taking this into account we can simplify eq B.4

$$\rho(q) = \rho(q,0,0) = \rho(l,0,0) = \sum_{s=0}^{N_g-1} \exp\left(i\frac{2\pi ls}{N_g}\right) n(s) \qquad (B.6)$$

where $n(s)$ represents a one-dimensional monomer distribution over the grid points along the x-axis. It is obtained by sorting monomers only according to their x-coordinates. Note that it can

dx.doi.org/10.1021/ma2007943 |Macromolecules 2011, 44, 5798–5816

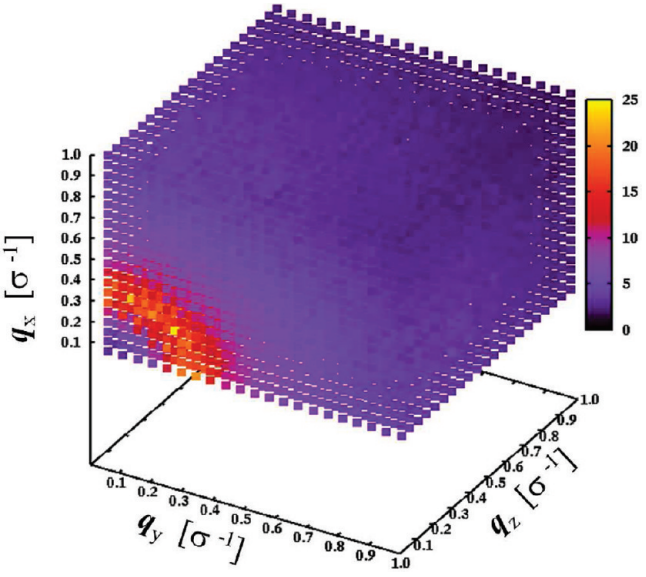

Figure 25. 3-D FFT from solution of fully charged polyelectrolyte chains with the degree of polymerization N = 300, chain bending constant K = 0, at polymer concentration c_p =5 × 10^{-3} σ^{-3} in salt-free regime.

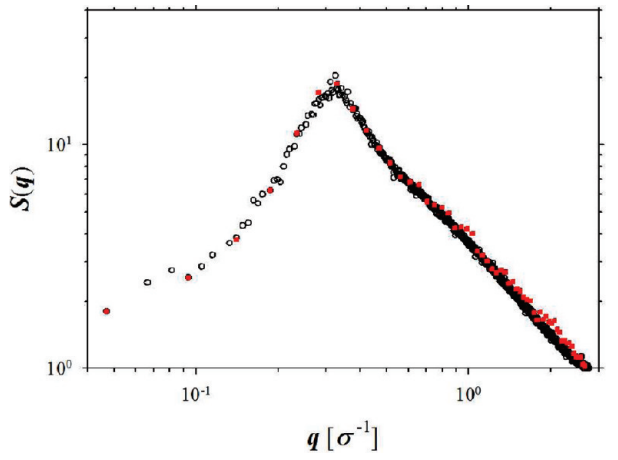

Figure 26. Scattering function $S(q)$ of fully charged polyelectrolyte chains with the degree of polymerization N = 300, chain bending constant K = 0, at polymer concentration c_p =5 × 10^{-3} σ^{-3} in salt-free solution calculated by using 3-D FFT (open circles) and 1-D FFT (red squares).

also be obtained from a 3-D monomer distribution function $n(s,j,k)$ by performing summations over indexes j and k. To improve accuracy, it is useful to perform FFT calculations for x, y, and z directions and average the final result for $S(q)$.

In Figure 26 we combined results for $S(q)$ obtained from 3-D FFT and 1-D FFT calculations. The results are close. However, it is important to point out that in the range of large q ($q \propto 2\pi/b$) the FFT-based methods introduce errors due to finite grid size.

■ ACKNOWLEDGMENT

The authors are grateful to the National Science Foundation for the financial support under Grant DMR-1004576.

■ REFERENCES

(1) Dobrynin, A. V.; Rubinstein, M. Theory of polyelectrolytes in solutions and at surfaces. *Prog. Polym. Sci.* **2005**, *30*, 1049–1118.

(2) Colby, R. H. Structure and linear viscoelasticity of flexible polymer solutions: comparison of polyelectrolyte and neutral polymer solutions. *Rheol. Acta* **2010**, *49* (5), 425–442.

(3) Dobrynin, A. V. Theory and simulations of charged polymers: From solution properties to polymeric nanomaterials. *Curr. Opin. Colloid Interface Sci.* **2008**, *13* (6), 376–388.

(4) Holm, C.; Joanny, J. F.; Kremer, K.; Netz, R. R.; Reineker, P.; Seidel, C.; Vilgis, T. A.; Winkler, R. G. Polyelectrolyte theory. *Adv. Polym. Sci.* **2004**, *166*, 67–111.

(5) Dobrynin, A. V.; Colby, R. H.; Rubinstein, M. Scaling theory of polyelectrolyte solutions. *Macromolecules* **1995**, *28* (6), 1859–1871.

(6) Forster, S.; Schmidt, M. Polyelectrolytes in Solution. *Adv. Polym. Sci.* **1995**, *120*, 51–133.

(7) Barrat, J. L.; Joanny, J. F. Theory of polyelectrolyte solutions. *Adv. Chem. Phys.* **1996**, *94*, 1–66.

(8) de Gennes, P. G.; Pincus, P.; Brochard, F.; Velasco, R. M. Remarks on polyelectrolyte conformation. *J. Phys. (Paris)* **1976**, *37*, 1461–1476.

(9) Yethiraj, A. Liquid State Theory of Polyelectrolyte Solutions. *J. Phys. Chem. B* **2009**, *113* (6), 1539–1551.

(10) Boris, D. C.; Colby, R. H. Rheology of sulfonated polystyrene solutions. *Macromolecules* **1998**, *31* (17), 5746–5755.

(11) Takahashi, A.; Kato, N.; Nagasawa, M. The osmotic pressure of polyelectrolyte in neutral salt solutions. *J. Phys. Chem.* **1970**, *74*, 944–946.

(12) Koene, R. S.; Nicolai, T.; Mandel, M. Scaling relations for aqueous polyelectrolyte-salt solutions. 3. Osmotic pressure as a function of molar mass and ionic strength in the semidilute regime. *Macromolecules* **1983**, *16*, 231–236.

(13) Raspaud, E.; da Conceicao, M.; Livolant, F. Do free DNA counterions control the osmotic pressure? *Phys. Rev. Lett.* **2000**, *84* (11), 2533–2536.

(14) Nagy, M. Thermodynamic study of aqueous solutions of polyelectrolytes of low and medium charge density without added salt by direct measurement of osmotic pressure. *J. Chem. Thermodyn.* **2010**, *42* (3), 387–399.

(15) Liao, Q.; Dobrynin, A. V.; Rubinstein, M. Molecular dynamics simulations of polyelectrolyte solutions: Osmotic coefficient and counterion condensation. *Macromolecules* **2003**, *36* (9), 3399–3410.

(16) Dobrynin, A. V.; Rubinstein, M.; Obukhov, S. P. Cascade of Transitions of Polyelectrolytes in Poor Solvent. *Macromolecules* **1996**, *29*, 2974–2979.

(17) Dobrynin, A. V.; Rubinstein, M. Hydrophobic polyelectrolytes. *Macromolecules* **1999**, *32* (3), 915–922.

(18) Solis, F. J.; de la Cruz, M. O. Variational approach to necklace formation in polyelectrolytes. *Macromolecules* **1998**, *31* (16), 5502–5506.

(19) Limbach, H. J.; Holm, C. Conformational properties of poor solvent polyelectrolytes. *Comput. Phys. Commun.* **2002**, *147* (1−2), 321–324.

(20) Limbach, H. J.; Holm, C.; Kremer, K. Conformations and solution structure of polyelectrolytes in poor solvent. *Macromol. Symp.* **2004**, *211*, 43–53.

(21) Limbach, H. J.; Holm, C. Single-chain properties of polyelectrolytes in poor solvent. *J. Phys. Chem. B* **2003**, *107* (32), 8041–8055.

(22) Chodanowski, P.; Stoll, S. Monte Carlo simulations of hydrophobic polyelectrolytes: Evidence of complex configurational transitions. *J. Chem. Phys.* **1999**, *111* (13), 6069–6081.

(23) Liao, Q.; Carrillo, J. M. Y.; Dobrynin, A. V.; Rubinstein, M. Rouse dynamics of polyelectrolyte solutions: Molecular dynamics study. *Macromolecules* **2007**, *40*, 7671–7679.

(24) Jeon, J.; Dobrynin, A. V. Necklace globule and counterion condensation. *Macromolecules* **2007**, *40*, 7695–7706.

(25) Lyulin, A. V.; Dunweg, B.; Borisov, O. V.; Darinskii, A. A. Computer simulation studies of a single polyelectrolyte chain in poor solvent. *Macromolecules* **1999**, *32* (10), 3264–3278.

(26) Baigl, D.; Ober, R.; Qu, D.; Fery, A.; Williams, C. E. Correlation length of hydrophobic polyelectrolyte solutions. *Europhys. Lett.* **2003**, *62* (4), 588–594.
(27) Spiteri, M. N.; Williams, C. E.; Boue, F. Pearl-necklace-like chain conformation of hydrophobic polyelectrolyte: a SANS study of partially sulfonated polystyrene in water. *Macromolecules* **2007**, *40* (18), 6679–6691.
(28) Aseyev, V. O.; Klenin, S. I.; Tenhu, H. Conformational changes of a polyelectrolyte in mixtures of water and acetone. *J. Polym. Sci., Part B: Polym. Phys.* **1998**, *36* (7), 1107–1114.
(29) Aseyev, V. O.; Klenin, S. I.; Tenhu, H.; Grillo, I.; Geissler, E. Neutron scattering studies of the structure of a polyelectrolyte globule in a water-acetone mixture. *Macromolecules* **2001**, *34* (11), 3706–3709.
(30) Morawetz, H. Revisiting some phenomena in polyelectrolyte solutions. *J. Polym. Sci., Part B: Polym. Phys.* **2002**, *40* (11), 1080–1086.
(31) Dobrynin, A. V.; Rubinstein, M. Hydrophobically modified polyelectrolytes in dilute salt-free solutions. *Macromolecules* **2000**, *33* (21), 8097–8105.
(32) Dobrynin, A. V. Molecular simulations of charged polymers. In *Simulation Methods for Polymers*; Kotelyanskii, M., Theodorou, D. N., Eds.; Marcel Dekker: New York, 2004; pp 259−312.
(33) Sarraguca, J. M. G.; Skepo, M.; Pais, A.; Linse, P. Structure of polyelectrolytes in 3: 1 salt solutions. *J. Chem. Phys.* **2003**, *119* (23), 12621–12628.
(34) Wei, Y. F.; Hsiao, P. Y. Role of chain stiffness on the conformation of single polyelectrolytes in salt solutions. *J. Chem. Phys.* **2007**, *127* (6), 064901.
(35) Wei, Y. F.; Hsiao, P. Y. Effect of chain stiffness on ion distributions around a polyelectrolyte in multivalent salt solutions. *J. Chem. Phys.* **2010**, *132* (2), 024905.
(36) Hsiao, P. Y.; Luijten, E. Salt-induced collapse and reexpansion of highly charged flexible polyelectrolytes. *Phys. Rev. Lett.* **2006**, *97* (14), 148301.
(37) Liu, S.; Ghosh, K.; Muthukumar, M. Polyelectrolyte solutions with added salt: A simulation study. *J. Chem. Phys.* **2003**, *119* (3), 1813–1823.
(38) Klos, J.; Pakula, T. Lattice Monte Carlo simulations of three-dimensional charged polymer chains. *J. Chem. Phys.* **2004**, *120* (5), 2496–2501.
(39) Klos, J.; Pakula, T. Computer simulations of a polyelectrolyte chain with a mixture of multivalent salts. *J. Phys.: Condens. Matter* **2005**, *17* (37), 5635–5645.
(40) Chang, R. W.; Yethiraj, A. Brownian dynamics simulations of salt-free polyelectrolyte solutions. *J. Chem. Phys.* **2002**, *116* (12), 5284–5298.
(41) Stevens, M. J.; Plimpton, S. J. The effect of added salt on polyelectrolyte structure. *Eur. Phys. J. B* **1998**, *2*, 341–345.
(42) Frenkel, D.; Smit, B. *Understanding Molecular Simulations*; Academic Press: New York, 2002.
(43) Stevens, M. J.; Kremer, K. The nature of flexible linear polyelectrolytes in salt-free solution - a molecular-dynamics study. *J. Chem. Phys.* **1995**, *103* (4), 1669–1690.
(44) Liao, Q.; Dobrynin, A. V.; Rubinstein, M. Molecular dynamics simulations of polyelectrolyte solutions: Nonuniform stretching of chains and scaling behavior. *Macromolecules* **2003**, *36* (9), 3386–3398.
(45) Grosberg, A. Y.; Khokhlov, A. R. *Statistical Physics of Macromolecules*; AIP Press: New York, 1994.
(46) Rubinstein, M.; Colby, R. H. *Polymer Physics*; Oxford University Press: New York, 2003.
(47) Oosawa, F. *Polyelectrolytes*; Marcel Dekker: New York, 1971.
(48) Chang, R.; Yethiraj, A. Osmotic pressure of salt-free polyelectrolyte solutions: A Monte Carlo simulation study. *Macromolecules* **2005**, *38* (2), 607–616.
(49) Fuoss, R. M.; Katchalsky, A.; Lifson, S. The potential of an infinite rod-like molecule and the distribution of counterions. *Proc. Natl. Acad. Sci. U.S.A.* **1951**, *37*, 579–586.
(50) Alfrey, T.; Berg, P. V.; Morawetz, H. The counterion distribution in solutions of rod-shaped polyelectrolytes. *J. Polym. Sci.* **1951**, *7*, 543–551.
(51) Keyser, U. F.; Koeleman, B. N.; S, v. D.; Krapf, D.; Smeets, R. M. M.; Lamy, S. G.; Dekker, N. H.; Dekker, C. Direct force measurements on DNA in a solid-stae nanopore. *Nature Phys.* **2006**, *2*, 473–477.
(52) Dobrynin, A. V.; Carrillo, J. M. Y. Swelling of biological and semiflexible polyelectrolytes. *J. Phys.: Condens. Matter* **2009**, *21* (42), 424112.
(53) Skolnick, J.; Fixman, M. Electrostatic persistence length of a wormlike polyelectrolyte. *Macromolecules* **1977**, *10* (5), 944–948.
(54) Odijk, T. Polyelectrolytes near the rod limit. *J. Polym. Phys., Part B: Polym. Phys.* **1977**, *15*, 477–483.
(55) Ullner, M. Comments on the scaling behavior of flexible polyelectrolytes within the Debye-Huckel approximation. *J. Phys. Chem. B* **2003**, *107* (32), 8097–8110.
(56) Fixman, M.; Skolnick, J. Polyelectrolyte excluded volume paradox. *Macromolecules* **1978**, *11*, 863–867.
(57) Odijk, T.; Houwaart, A. C. On the theory of the excluded-volume effect of a polelectrolyte in a 1−1 electrolyte solution. *J. Polym. Sci., Polym. Phys. Ed.* **1978**, *16*, 627–639.
(58) Muthukumar, M. Adsorption of a polyelectrolyte chain to a charged surface. *J. Chem. Phys.* **1987**, *86* (12), 7230–7235.
(59) Muthukumar, M. Double screening in polyelectrolyte solutions: Limiting laws and crossover formulas. *J. Chem. Phys.* **1996**, *105* (12), 5183–5199.
(60) Gubarev, A.; Carrillo, J. M. Y.; Dobrynin, A. V. Scale-Dependent Electrostatic Stiffening in Biopolymers. *Macromolecules* **2009**, *42* (15), 5851–5860.
(61) Fixman, M. The flexibility of polyelectrolyte molecules. *J. Chem. Phys.* **1982**, *76*, 6346–6353.
(62) Everaers, R.; Milchev, A.; Yamakov, V. The electrostatic persistence length of polymers beyond the OSF limit. *Eur. Phys. J. E* **2002**, *8* (1), 3–14.
(63) Nguyen, T. T.; Shklovskii, B. I. Persistence length of a polyelectrolyte in salty water: Monte Carlo study. *Phys. Rev. E* **2002**, *66* (2), 021801−1−7.
(64) Le Bret, M. Electrostatic contribution of the persistence length of a polyelectrolyte. *J. Chem. Phys.* **1982**, *76*, 6243–6255.
(65) Borsali, R.; Rinaudo, M.; Noirez, L. Light-scattering and small-angle neutron-scattering from polyelectrolyte solutions - the succinoglycan. *Macromolecules* **1995**, *28* (4), 1085–1088.
(66) Vallat, P.; Catala, J. M.; Rawiso, M.; Schosseler, F. Flexible conjugated polyelectrolyte solutions: A small angle scattering study. *Macromolecules* **2007**, *40* (10), 3779–3783.
(67) Nishida, K.; Urakawa, H.; Kaji, K.; Gabrys, B.; Higgins, J. S. Electrostatic persistence length of NaPSS polyelectrolytes determined by a zero average contrast SANS technique. *Polymer* **1997**, *38* (24), 6083–6085.
(68) Buhler, E.; Boue, F. Chain persistence length and structure in hyaluronan solutions: Ionic strength dependence for a model semirigid polyelectrolyte. *Macromolecules* **2004**, *37* (4), 1600–1610.
(69) Essafi, W.; Spiteri, M. N.; Williams, C. E.; Boue, F. Hydrophobic polyelectrolytes in better polar solvent. Structure and chain conformation as seen by SAXS and SANS. *Macromolecules* **2009**, *42*, 9568–9580.
(70) Prabhu, V. M.; Amis, E. J.; Bossev, D. P.; Rosov, N. Counterion associative behavior with flexible polyelectrolytes. *J. Chem. Phys.* **2004**, *121* (9), 4424–4429.
(71) Wang, D. L.; Lal, J.; Moses, D.; Bazan, G. C.; Heeger, A. J. Small angle neutron scattering (SANS) studies of a conjugated polyelectrolyte in aqueous solution. *Chem. Phys. Lett.* **2001**, *348* (5−6), 411–415.
(72) Boucard, N.; David, L.; Rochas, C.; Montembault, A.; Viton, C.; Domard, A. Polyelectrolyte microstructure in chitosan aqueous and alcohol solutions. *Biomacromolecules* **2007**, *8* (4), 1209–1217.
(73) Combet, J.; Isel, F.; Rawiso, M.; Boue, F. Scattering functions of flexible polyelectrolytes in the presence of mixed valence counterions: Condensation and scaling. *Macromolecules* **2005**, *38* (17), 7456–7469.
(74) Ermi, B. D.; Amis, E. J. Domain structures in low ionic strength solutions. *Macromolecules* **1998**, *31*, 7378–7384.

(75) Spiteri, M. N.; Boue, F.; Lapp, A.; Cotton, J. P. Polyelectrolyte persistence length in semidilute solution as a function of the ionic strength. *Physica B* **1997**, *234*, 303–305.

(76) Chang, R. W.; Yethiraj, A. Brownian dynamics simulations of polyelectrolyte solutions with divalent counterions. *J. Chem. Phys.* **2003**, *118* (24), 11315–11325.

(77) Ermoshkin, A. V.; de la Cruz, M. O. Polyelectrolytes in the presence of multivalent ions: Gelation versus segregation. *Phys. Rev. Lett.* **2003**, *90* (12), 125504-1-4.

(78) Ermoshkin, A. V.; De la Cruz, M. O. Gelation in strongly charged polyelectrolytes. *J. Polym. Sci., Part B: Polym. Phys.* **2004**, *42* (5), 766–776.

(79) Gonzalez-Mozuelos, P.; de la Cruz, M. O. Association in electrolyte solutions: Rodlike polyelectrolytes in multivalent salts. *J. Chem. Phys.* **2003**, *118* (10), 4684–4691.

(80) Huang, C. I.; de la Cruz, M. O. Polyelectrolytes in multivalent salt solutions: Monomolecular versus multimolecular aggregation. *Macromolecules* **2002**, *35* (3), 976–986.

(81) Raspaud, E.; de la Cruz, M. O.; Sikorav, J. L.; Livolant, F. Precipitation of DNA by polyamines: A polyelectrolyte behavior. *Biophys. J.* **1998**, *74* (1), 381–393.

(82) Plimpton, S. J. Fast parallel algorithms for short-range molecular dynamics. *J. Comput. Phys.* **1995**, *117* (1), 1-19. http://lammps.sandia.gov.